JEM Journal of Experimental Medicine

ARTICLE

Widespread B cell perturbations in HIV-1 infection afflict naive and marginal zone B cells

Thomas Liechti[1], Claus Kadelka[1,2], Dominique L. Braun[1,2], Herbert Kuster[1,2], Jürg Böni[1], Melissa Robbiani[3], Huldrych F. Günthard[1,2], and Alexandra Trkola[1]

Perturbations in B cells are a hallmark of HIV-1 infection. This is signified by increased numbers of exhausted CD21^{neg} memory B cells, driven by continuous antigen-specific and bystander activation. Using high-dimensional flow cytometry, we demonstrate that this exhausted phenotype is also prevalent among peripheral antigen-inexperienced naive and marginal zone (MZ) B cells in acute and chronic HIV-1 infection. A substantial fraction of naive and MZ B cells exhibit down-regulated CD21 levels and diminished response to B cell receptor (BCR)–dependent stimulation. Compared with CD21^{pos} subsets, the CD21^{neg} naive and MZ B cells differ in the expression of chemokine receptors and activation markers. Effective antiretroviral treatment normalizes peripheral naive and MZ B cell populations. Our results emphasize a more widely spread impairment of B cells in HIV-1 infection than previously appreciated, including antigen-inexperienced cells. This highlights the importance of monitoring functional capacities of naive B cells in HIV-1 infection, as exhausted CD21^{neg} naive B cells may severely impair induction of novel B cell responses.

Introduction

HIV-1 infection is accompanied by massive bystander activation, impairing many components of the immune system, including B cells (Bangs et al., 2006; Haas et al., 2011). These perturbations lead to a general deficiency in mounting antibody responses against pathogens and vaccines during HIV-1 infection (Malaspina et al., 2005; Titanji et al., 2006; Fritz et al., 2010; Kernéis et al., 2014). Neutralizing antibodies against HIV-1 emerge within months after infection but are subject to rapid escape by the virus (Wei et al., 2003; Bunnik et al., 2008). In a minority of HIV-1–infected patients, continuous virus and antibody coevolution leads to the development of antibodies with improved potency and breadth, so-called broadly neutralizing antibodies (bnAbs; Moore et al., 2012; Liao et al., 2013). What effect B cell perturbations have on the development of HIV-1 neutralizing antibodies and bnAbs remains uncertain (Derdeyn et al., 2014; Meffre et al., 2016). While a number of factors have been suggested to shape the development of bnAbs (Doria-Rose et al., 2010; Moore et al., 2015; Rusert et al., 2016; Kadelka et al., 2018; Subbaraman et al., 2018), disturbed functionality of the B cell population may be an additional reason that bnAbs develop late and only in a fraction of individuals (Derdeyn et al., 2014; Meffre et al., 2016). Likewise, certain alterations of the immune environment that also affect B cells may foster bnAb evolution (Kadelka et al., 2018; Subbaraman et al., 2018).

Perturbations of B cells in HIV-1 infection are characterized by increased frequencies of activated (AM) and exhausted tissue-like (TLM) memory B cells. These cells differ from resting (RM) and intermediate (IM) memory B cells by the loss of complement receptor 2 (CD21) expression; distinct expression of activation, inhibitory, and chemokine receptors; and diminished response to stimulation (Moir et al., 2008; Moir and Fauci, 2013; Kardava et al., 2014). Beyond shifts within memory B cells, increased frequencies of plasmablasts and transitional B cells have been observed (Malaspina et al., 2006; Buckner et al., 2013). A substantial proportion of HIV-1–specific memory B cells are found within TLM B cells (Kardava et al., 2014). This suggests that a large fraction of HIV-1–specific B cells are exhausted and impaired in generating effective high-affinity antibody responses (Kardava et al., 2014; Meffre et al., 2016).

De novo antibody responses are diminished in HIV-1 infection (Malaspina et al., 2005; Titanji et al., 2006; Fritz et al., 2010; Kernéis et al., 2014). We therefore hypothesized that HIV-1 may

[1]Institute of Medical Virology, University of Zurich, Zurich, Switzerland; [2]Division of Infectious Diseases and Hospital Epidemiology, University Hospital Zurich, Zurich, Switzerland; [3]Center for Biomedical Research, Population Council, New York, NY.

Correspondence to Alexandra Trkola: trkola.alexandra@virology.uzh.ch; T. Liechti's present address is ImmunoTechnology Section, Vaccine Research Center, National Institute of Allergy and Infectious Diseases, National Institutes of Health, Bethesda, MD; C. Kadelka's present address is Department of Mathematics, Iowa State University, Ames, IA.

also impact antigen-inexperienced naive B cells. We applied high-dimensional flow cytometry to comprehensively assess the longitudinal phenotypic and functional dynamics of B cell subsets in blood during acute and chronic HIV-1 infection and probed the potential of antiretroviral therapy (ART) in reversing these alterations. We demonstrate that CD21^{neg} naive and CD21^{neg} MZ B cell subsets emerge early during acute HIV-1 infection, increase in frequency during chronic infection, and regress upon ART. The phenotype and functionality of CD21^{neg} naive and CD21^{neg} MZ B cells resembles anergic polyreactive naive B cells described in autoimmunity (Rakhmanov et al., 2009; Isnardi et al., 2010; Tipton et al., 2015; Flint et al., 2016). This highlights the need to investigate their role in the development of polyreactive HIV-1–specific antibody responses (Mouquet et al., 2010; Liu et al., 2015). Importantly, our findings emphasize the profound influence of HIV-1 replication at early stages of B cell maturation that result in the induction of an anergic state. This may be a driving force of the delayed and impaired antibody responses observed in HIV-1 infection.

Results

Longitudinal changes of major B cell subsets in HIV-1 and the impact of ART

To investigate if HIV-1 induces widespread perturbation of B cells, we analyzed peripheral blood from HIV-1–infected individuals enrolled in the Zurich Primary HIV Infection Study (ZPHI) using high-dimensional flow cytometry. Patients were stratified into two groups according to the time point of ART initiation. In the early ART initiation group, ART was initiated during acute infection, followed by a period of ART interruption during chronic phase. In the late ART initiation group, ART was delayed and initiated during chronic infection (Fig. 1 A and Tables S1 and S2). For each HIV-1–infected individual, four time points encompassing (i) acute infection, (ii) 1 yr and (iii) 2 yr of chronic infection, and (iv) 1 yr on ART were analyzed. Table S2 describes the selection of early and late ART group samples for the various analyses. Healthy controls from single sampling time points were used as baseline.

We used 16-color flow cytometry to define main B cell subsets (transitional, naive, marginal zone [MZ], memory B cells, and plasmablasts) and memory B cell subsets in blood (Fig. S1, A and B; Liechti et al., 2018a). By monitoring changes in B cell subsets during HIV-1 infection, we found increased frequencies of transitional B cells and plasmablasts in HIV-1–infected individuals (n = 19) compared with healthy donors (n = 29; Fig. 1 B). In contrast, patients on ART exhibited significantly ($P < 0.01$) higher frequencies of naive B cells than during their acute phase. Importantly, ART treatment reversed the elevated frequencies of transitional B cell and plasmablasts to healthy donor levels.

In accordance with earlier reports (Moir et al., 2008, 2010), memory B cell subsets were distorted, showing increased frequencies of AM and TLM B cells in contrast to decreased levels of IM and RM B cells during acute and chronic HIV-1 infection (Fig. 1 C). ART did not restore these subsets to levels observed in healthy individuals (Fig. 1 C; Moir et al., 2010). Loss of CD21 signifies AM and TLM B cells in HIV-1 infection (Moir et al., 2008; Moir and Fauci, 2013). Strikingly, we also observed increased frequencies of CD21^{neg} naive and MZ B cells (Fig. 1 D and Fig. S1 B). Successful ART restored CD21^{pos} subset levels, albeit not to frequencies observed in healthy donors. The influence of HIV-1 infection on antigen-inexperienced B cells demonstrated by the loss of CD21^{pos} naive and MZ B cells is highly intriguing and underscores the general impact of HIV-1 infection on B cells.

We next assessed the potential influences of ART initiation and disease course, analyzing B cell subsets in the early ART and late ART groups (Fig. S1, B–D). With the exception of MZ B cell levels, which were lower in the acute-phase sampling time point in the early ART initiation group, no differences between the two treatment groups were observed (Fig. S2, A–C). Healthy controls (n = 29) and individuals from the late ART initiation group (n = 8) showed similar MZ B cell levels, while patients within the early ART initiation group (n = 11) had reduced MZ B cell frequencies (Fig. S2 A). Interestingly, samples we had available for the early ART group were derived sooner after infection compared with the late ART group (Tables S1 and S2). Collectively, this strongly suggests that MZ B cells are disturbed very early during acute HIV-1 infection but that their frequency rapidly normalizes (Fig. S2 D).

Assessing B cell subset signatures

We next performed a signature analysis to explore if HIV-1 infection leads to the formation of distinct phenotypic patterns. We focused therein on distinct subsets and thus did not include total naive, MZ, and memory B cells in the analysis. Data on B cell subsets from healthy controls (n = 29) and HIV-1–infected individuals (n = 19 for acute time point; n = 21 for chronic 2 yr time point and after 1 yr of ART; Fig. 1, B–D) were analyzed using the dimensionality reduction algorithm tSNE (t-distributed stochastic neighbor embedding; Fig. 1 E). The tSNE-based B cell signatures of viremic samples from HIV-1 patients (acute and chronic time points) proved distinct from signatures observed for healthy controls and samples after prolonged ART highlighting the influence of HIV-1 replication (Fig. 1 E).

Four of the chronic HIV-1–infected individuals (Z23, Z32, Z58, and Z92) displayed patterns that closely matched healthy controls. This reflected their overall low HIV-1 progression as evidenced by lower viral loads, higher CD4 counts, and lower plasma IgG levels (Fig. 1, E and F). We next probed the impact of viral load, CD4 count, and plasma IgG levels on the emergence of CD21^{neg} naive and CD21^{neg} MZ B cells. We observed no direct link between levels of CD21^{neg} naive B cells and these parameters in acute or chronic infection (Fig. 2). However, the increase of CD21^{neg} MZ B cells was strongly linked with decreasing CD4 T cell counts and increases in viral load, but not plasma IgG levels during the chronic phase (Fig. 2). We next explored associations between CD21^{neg} naive and CD21^{neg} MZ B cells and the HIV-1–specific IgG1 response in a subset of patients (acute, n = 13; chronic 2 yr, n = 14). IgG1 reactivity with 13 HIV-1 antigens was measured in a multiplex binding assay as recently described (Kadelka et al., 2018; Liechti et al., 2018b). Interestingly, CD21^{neg} naive B cells, but not CD21^{neg} MZ B cells, correlated positively with HIV-1–specific antibody responses to eight antigens in acute and two antigens in chronic infection (Fig. S3).

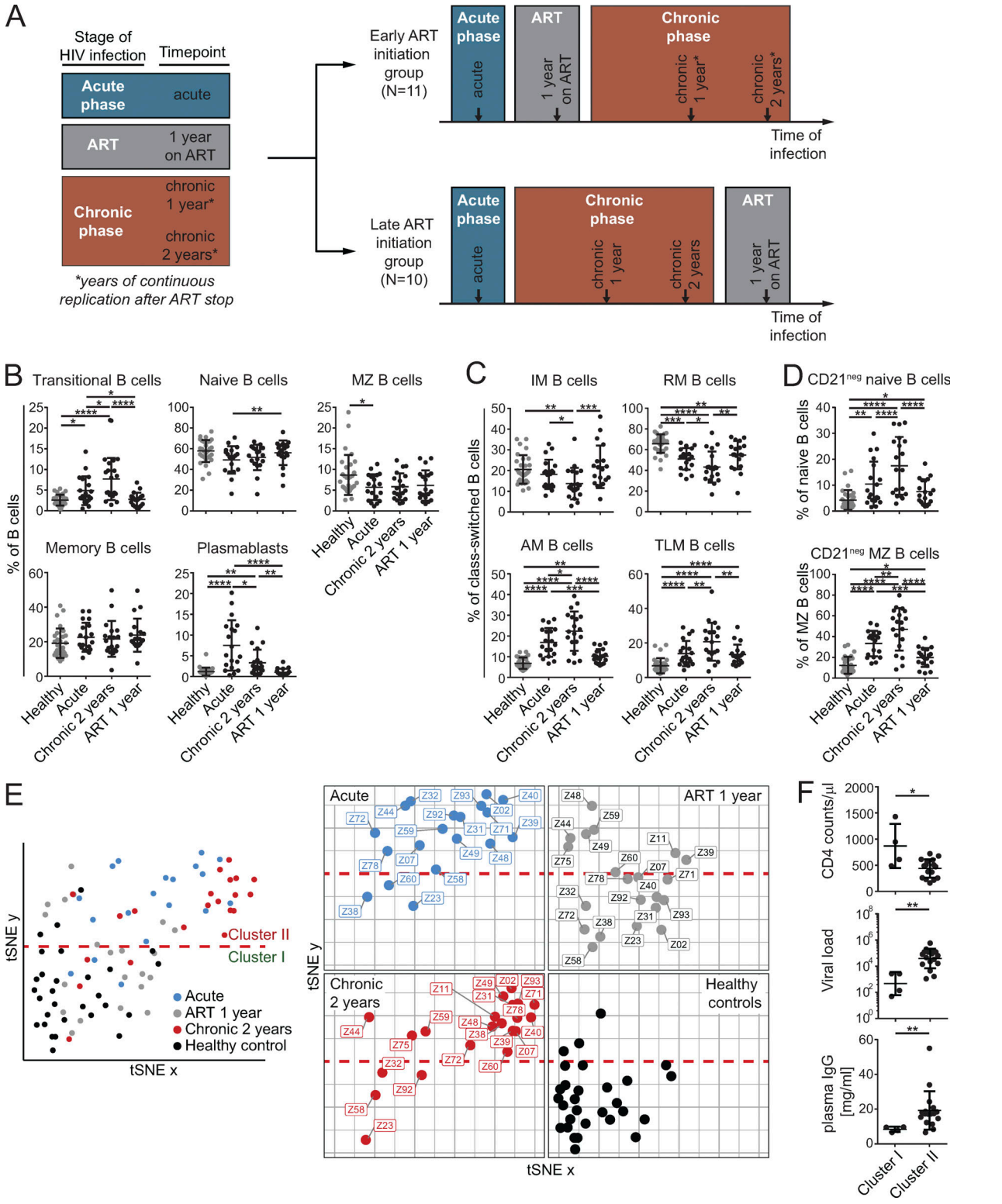

Figure 1. **B cell subset changes during HIV-1 infection. (A)** Schematic overview of the longitudinal HIV-1 study (see Materials and methods). **(B–D)** Frequencies of main B cell subsets (B), memory B cell subsets (C), and CD21^{neg} naive and CD21^{neg} MZ B cells (D) from healthy donors (n = 29) and HIV-1–infected patients (n = 19) at acute and chronic disease stages and after 1 yr on ART. P values were derived from linear mixed-effect models with Tukey's method for multiple comparison (see Materials and methods). **(E)** Left: Two-dimensional tSNE map of healthy donors (n = 29) and patients (n = 19 for acute and n = 21 for ART 1-yr and chronic 2-yr time points) based on the z-scores of the frequencies of B cell subsets shown in B–D (see Materials and methods). Right: Stratification of the same tSNE map by time point and healthy controls. The red dashed line separates cluster I (bottom) and II (top). **(F)** Clinical parameters of chronic HIV-1–infected individuals (n = 20 for CD4 counts and n = 21 for plasma IgG and viral load) in cluster I and cluster II (from E) compared using Mann–Whitney U test. Data represent a single measurement from each patient time point assessed. *, P < 0.05; **, P < 0.01; ***, P < 0.001; ****, P < 0.0001. Error bars in B–D and F indicate SD.

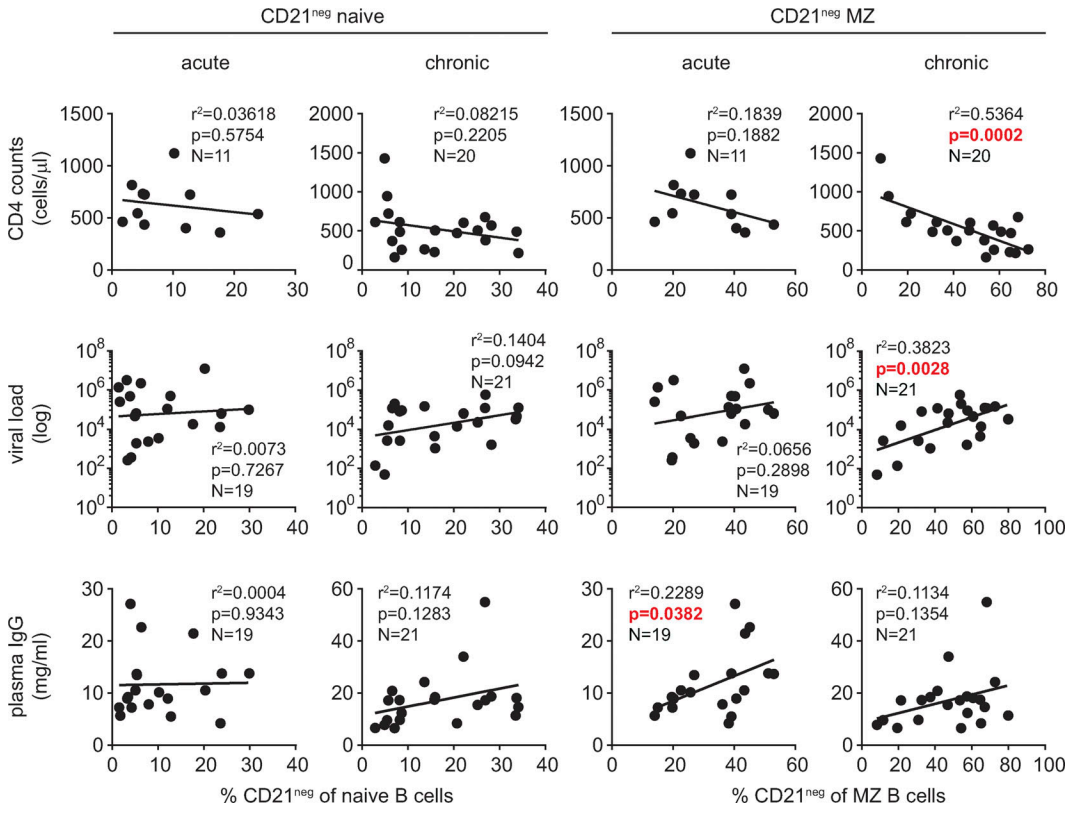

Figure 2. **Correlation of CD21^{neg} naive and CD21^{neg} MZ B cells with clinical parameters.** Linear regression of CD21^{neg} naive and CD21^{neg} MZ B cells with CD4 counts, viral load, and plasma IgG concentration in acute and chronic HIV-1 infection. Sample size N, coefficient of determination r^2, and P values are indicated. P < 0.05 was considered statistically significant and is highlighted in red. Data represent single measurements from each patient time point assessed.

Our analysis did not have the statistical power to define antigen-specific IgG patterns and dependencies. However, the observation that B cell subset– and disease stage–driven effects on IgG1 levels can occur highlights the need to resolve the impact on responses to different HIV-1 antigens as well as neutralizing antibodies in forthcoming studies.

Differential expression of chemokine receptors and IL-21R on CD21^{neg} and CD21^{pos} naive and MZ B cell subsets

CD21^{neg} B cells in autoimmune and chronic viral diseases display altered chemokine and cytokine receptor expression profiles (Rakhmanov et al., 2009; Isnardi et al., 2010; Saadoun et al., 2013; Moir and Fauci, 2014; Tipton et al., 2015). To explore if this extends to naive and MZ B cell subsets, we analyzed the expression of CCR7, CXCR3, CXCR4, CXCR5, and IL-21R in healthy (n = 29) and chronically HIV-1–infected (n = 21) donors (Figs. 3 and 4). CD21^{neg} naive B cells generally displayed decreased frequencies of CCR7, CXCR5, and IL-21R and an increased frequency of CXCR3-expressing cells (Fig. 3, A and B). Receptor levels on these subsets differed accordingly (Fig. 4, A and B). With the exception of IL-21R, the same alterations in expression profiles were observed between CD21^{neg} and CD21^{pos} MZ B cells (Fig. 3 B and Fig. 4, A and B). IL-21R was expressed at higher levels and on more cells within the CD21^{neg} MZ B cell subset in chronically HIV-1–infected, but not healthy, individuals. The divergent expression dynamics of IL-21R in CD21^{neg} naive and CD21^{neg} MZ B cells in HIV-1 infection is intriguing and may reflect differential dependence on IL-21R signaling.

HIV-1 infection was signified by a decrease in CCR7 and CXCR5 and an increase in CXCR3 and IL-21R-expressing CD21^{neg} and CD21^{pos} naive B cell subsets (Fig. 3 C). A similar pattern was observed for MZ B cells, with the exception of CCR7 expression, which was elevated in CD21^{neg} MZ B cells during HIV-1 infection (Fig. 3 C). Comparison of expression levels in CD21^{neg} and CD21^{pos} naive and CD21^{neg} and CD21^{pos} MZ B cells between healthy and chronic HIV-infected individuals confirmed these observations (Fig. 4, B and C).

Healthy individuals displayed fewer CXCR4-expressing cells among CD21^{neg} naive and MZ B cells compared with the corresponding CD21^{pos} subsets (Fig. 3 B). This pattern differed in chronic HIV-1 infection. CD21^{neg} and CD21^{pos} naive B cells expressed CXCR4 at similar frequencies, and the contingency of CXCR4^{pos} CD21^{neg} MZ B cells was higher than in CD21^{pos} MZ B cells (Fig. 3 B). In line with this, we observed an overall increase in CXCR4 expression in CD21^{neg} compared with CD21^{pos} B cell subsets (Fig. 4, B and C). Of note, CD21^{neg} naive and CD21^{neg} MZ B cells of HIV-1–infected donors displayed increased CD19 expression levels (Fig. 4, B and C), as described for exhausted B cells in autoimmunity (Rakhmanov et al., 2009).

We next explored longitudinal changes in phenotypes of CD21^{neg} naive and CD21^{neg} MZ B cells upon prolonged exposure to HIV-1, comparing subset patterns in the early (n = 11) and late (n = 8) ART initiation groups (Fig. 5 A). The most pronounced

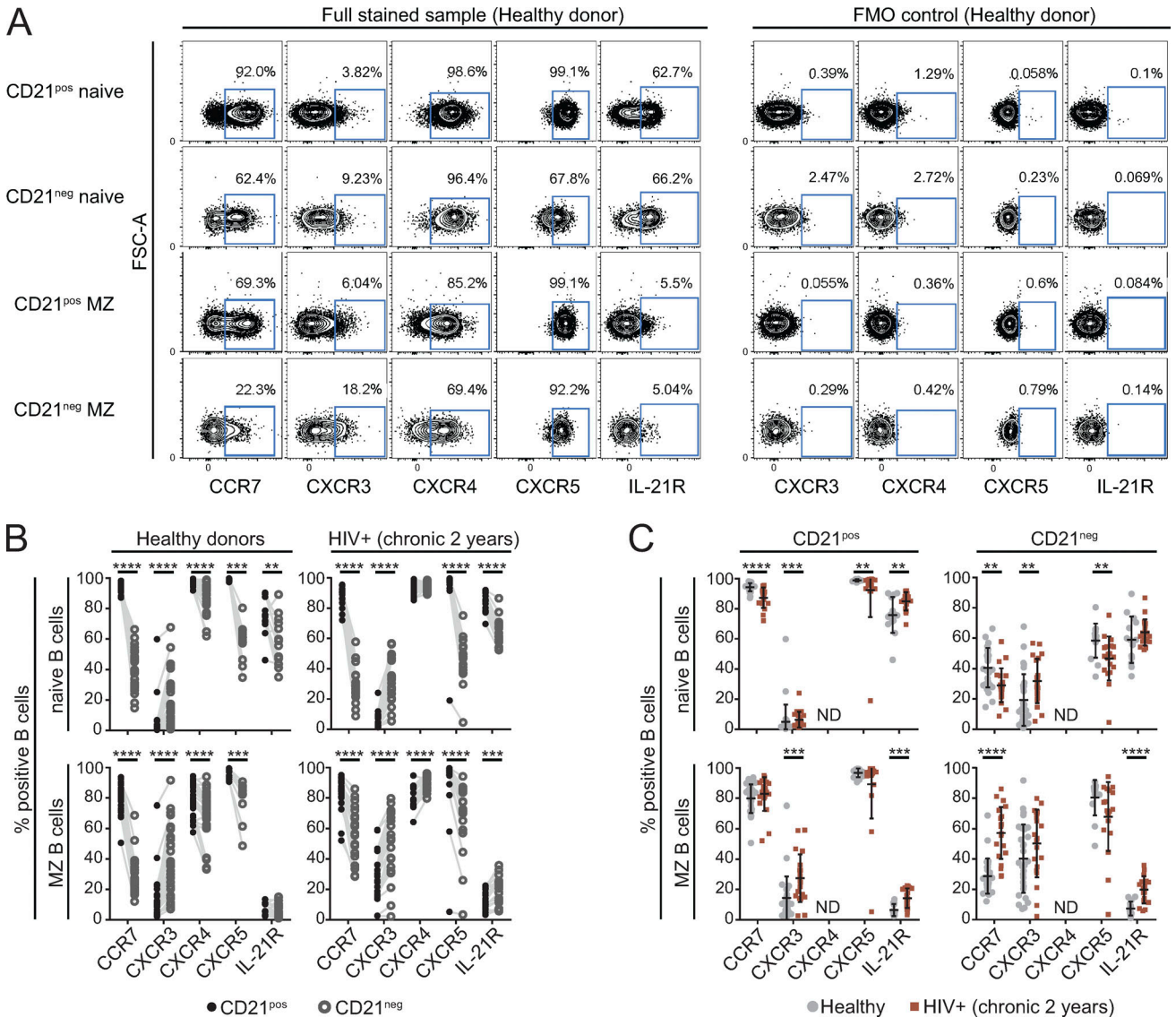

Figure 3. **Phenotype of CD21^{neg} naive and CD21^{neg} MZ B cells. (A)** Expression of CCR7, CXCR3, CXCR4, CXCR5, and IL-21R on CD21^{neg} and CD21^{pos} naive and CD21^{neg} and CD21^{pos} MZ B cells and FMO controls are shown for a representative healthy control donor. Numbers in dot plots indicate percentage of gated population. **(B)** Comparison of frequencies of CD21^{neg} (gray open circle) and CD21^{pos} (black closed circle) naive and MZ B cells expressing CCR7, CXCR3, CXCR4, CXCR5, and IL-21R in healthy (n = 29) and HIV-1–infected (chronic 2 yr, n = 21) donors. **(C)** Differences of the same markers between healthy donors (n = 29, n = 14 for IL-21R and CXCR5) and chronically HIV-1–infected donors (chronic 2 yr, n = 21, n = 19 for IL-21R and CXCR5) are shown. Data represent single measurements from each patient time point assessed. Comparison between CD21^{neg} and CD21^{pos} naive and CD21^{neg} and CD21^{pos} MZ B cells within the same individual was done using Wilcoxon signed rank test and between healthy and HIV-1–infected individuals using Mann–Whitney U test. ND, comparison not performed (see Materials and methods). **, P < 0.01; ***, P < 0.001; ****, P < 0.0001.

pattern changes were observed among the early ART initiation group during continued virus replication (Fig. 5, A and B). This again reflects an impact of continued virus replication on the phenotype of CD21^{neg} naive B cells and MZ cells. Overall, we observed more variation among B cell phenotypes in the early ART group, where individuals went through chronic infection stages only upon ART cessation. In contrast, uninterrupted virus replication, as monitored in the late ART initiation group, appeared to lead to a set-point level in B cell perturbation that late ART could not fully reverse. Collectively, our data therefore reveal distinct phenotypes of CD21^{neg} naive and CD21^{neg} MZ B cells, which are differentially impacted by HIV-1 infection.

CD21^{neg} naive B cells form a heterogeneous population

To obtain a complete overview of the subset heterogeneity, we subjected our data to an unsupervised spanning-tree progression analysis of density-normalized events (SPADE) clustering analysis (Qiu et al., 2011), followed by Ward hierarchical clustering. We focused the analysis on CD21^{neg} naive B cells, because the numbers of CD21^{neg} MZ B cells were too low to allow reliable clustering. Longitudinal samples (acute, chronic 1 yr, chronic 2 yr, and ART 1 yr) of 17 HIV-1–infected patients and 15 healthy donors were assessed. The SPADE analysis provided an intriguing insight into the high diversity within CD21^{neg} naive B cells (Fig. 6, A and B). CXCR4 was not chosen for clustering due

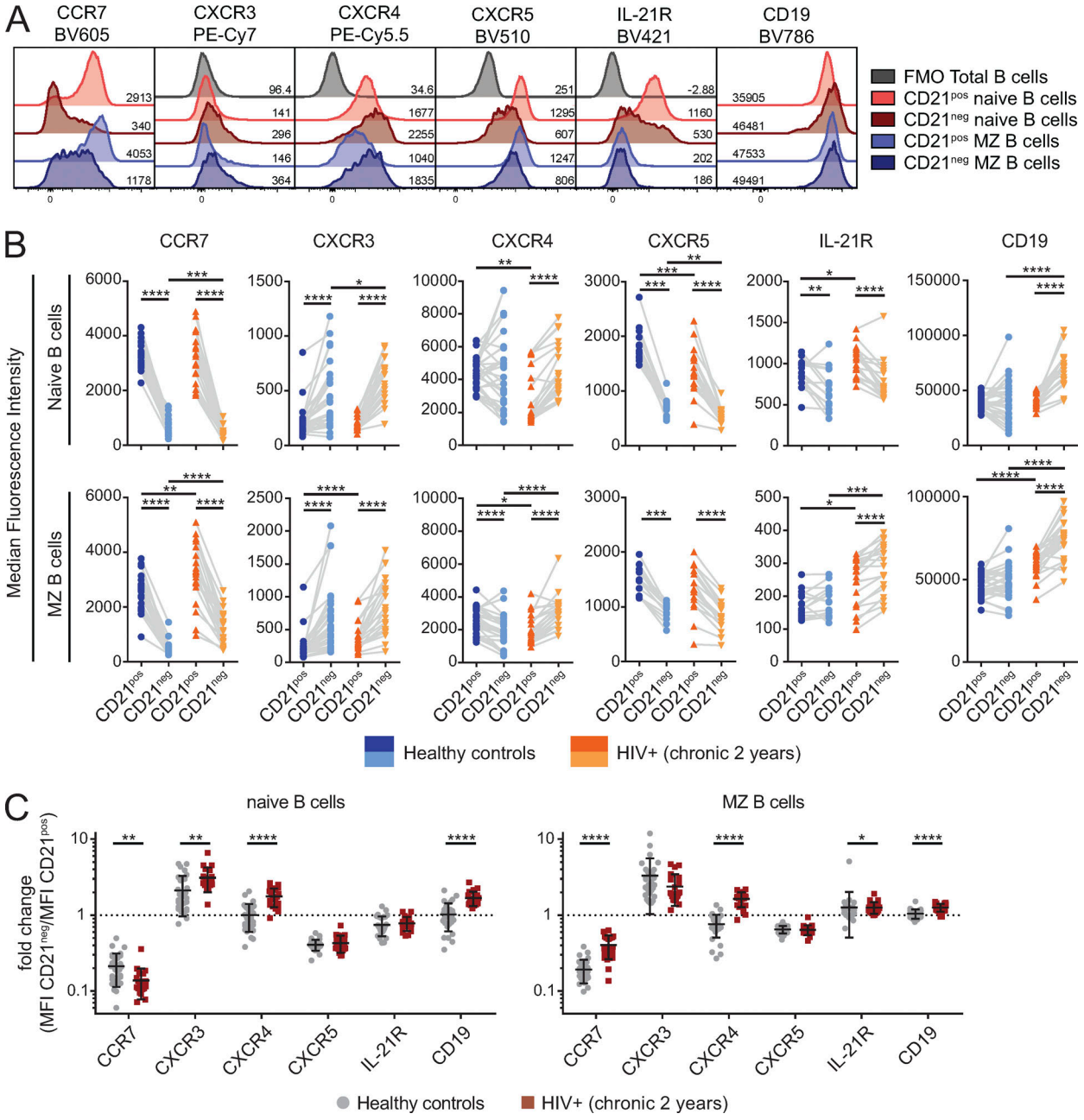

Figure 4. **CD21^{neg} naive and CD21^{neg} MZ B cells exhibit distinct expression levels of chemokine receptors IL-21R and CD19. (A)** Histogram overlays of CCR7, CXCR3, CXCR4, CXCR5, IL-21R, and CD19 expression on CD21^{neg} and CD21^{pos} naive (dark red and red, respectively) and CD21^{neg} and CD21^{pos} MZ B cells (dark blue and blue, respectively) from a chronic HIV-1–infected patient are shown. Where applied, FMO controls (gray) from a healthy donor are depicted. Numbers in histogram overlay indicate the MFI. **(B)** Differences of MFI between CD21^{neg} and CD21^{pos} naive (top row) and CD21^{neg} and CD21^{pos} MZ B cells (bottom row) in healthy controls (n = 29, n = 14 for IL-21R and CXCR5) and HIV-1–infected patients (chronic 2 yr, n = 21, n = 19 for IL-21R and CXCR5) are shown for CCR7, CXCR3, CXCR4, CXCR5, IL-21R, and CD19. **(C)** MFI fold-change ratio between CD21^{neg} and CD21^{pos} naive or CD21^{neg} and CD21^{pos} MZ B cells for CCR7, CXCR3, CXCR4, CXCR5, IL-21R, and CD19 are shown and compared between healthy controls (n = 29) and chronically HIV-1–infected patients (n = 21). Data represent single measurements from each patient time point assessed. Wilcoxon signed rank test was used to compare CD21^{neg} and CD21^{pos} naive and CD21^{neg} and CD21^{pos} MZ B cells within the same individual, and Mann–Whitney U test to compare differences between healthy controls and chronically HIV-1–infected patients. *, P < 0.05; **, P < 0.01; ***, P < 0.001; ****, P < 0.0001. Error bars indicate SD.

to staining variability across samples (see Materials and methods). Likewise, owing to its unimodal expression pattern, CD19 was not selected for cluster formation. However, some expression profiles of markers used for clustering (for example, high levels of CXCR3 in Ward clusters 3, 4, and 8) were associated with elevated levels of CD19 and CXCR4 and highlighted some degree of redundancy of these markers (Fig. 6, A–C). A drawback of clustering algorithms is the need for overclustering to define rare cell subsets (Diggins et al., 2015; Nowicka et al., 2017). We thus subsequently merged SPADE clusters with similar median

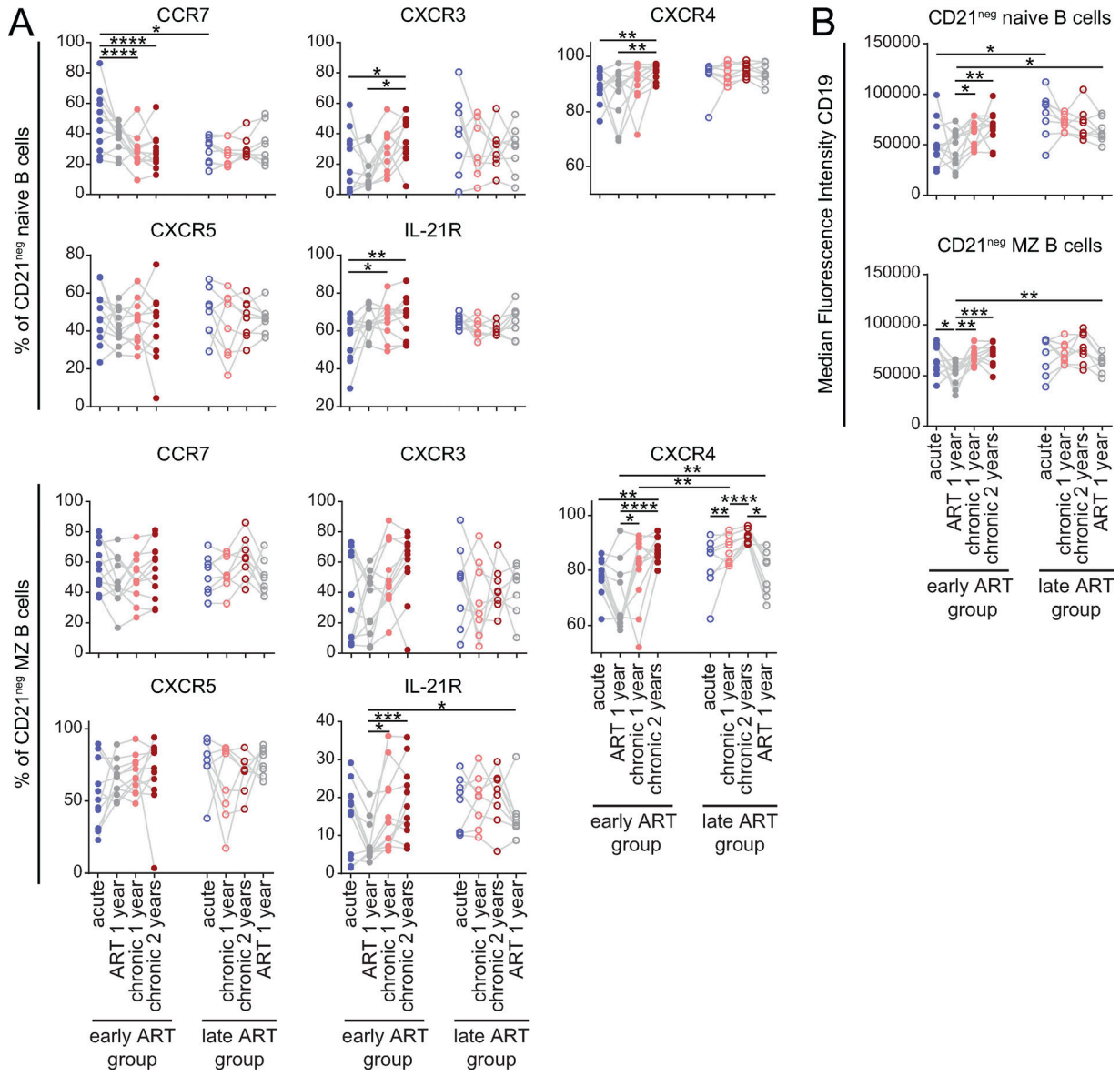

Figure 5. **Longitudinal analysis of phenotypic markers on CD21^{neg} naive and CD21^{neg} MZ B cells. (A)** Longitudinal analysis of percentage of CD21^{neg} naive and CD21^{neg} MZ B cells expressing CCR7, CXCR3, CXCR4, CXCR4, and IL-21R. HIV-1–infected patients were split into an early ART initiation group (closed circles; n = 11) and a late ART initiation group (open circles, n = 8). **(B)** Expression levels of CD19 on CD21^{neg} naive and CD21^{neg} MZ B cells for the same samples are depicted. Data represent single measurements from each patient time point assessed. P values were derived from linear mixed-effect models with Tukey's method for multiple comparison (see Materials and methods). *, P < 0.05; **, P < 0.01; ***, P < 0.001; ****, P < 0.0001.

expression levels using Ward's hierarchical clustering method (Ward, 1963) and defined 10 distinct clusters (Fig. 6 C). To verify the validity of the Ward clustering, we performed a manual analysis of these 10 Ward clusters, which confirmed distinct expression patterns for the majority of them (Fig. 6 C). Of note, some Ward clusters shared common phenotypic characteristics such as high CXCR3 levels (clusters 2, 3, and 8), high IL-21R levels (clusters 4, 6, and 9), or high CCR7 and CXCR5 levels (clusters 7, 8, and 10; Fig. 7 A).

We next analyzed the longitudinal dynamics of these clusters during HIV-1 infection by stratifying the early and late ART initiation groups and comparing them with healthy controls (Fig. 7, A and B). Overall, Ward clusters of HIV-1–infected and healthy controls were similar. Of note, as observed in the manual analysis (Fig. 6), longitudinal changes of the identified Ward subsets were apparent only in the early ART group and restricted to clusters 4, 7, and 10 (Fig. 7 B). Cluster 4 was associated with higher IL-21R and CXCR3 expression, whereas clusters 7 and 10 were associated with high expression of CCR7 and CXCR5 (Fig. 7 A). The longitudinal changes observed for clusters 4, 7, and 10 were most pronounced at 2 yr of chronic infection, the latest time point measured in our study, emphasizing the progressive effect of prolonged HIV-1 infection. Concomitant with decreased CCR7 levels, an increase in cell subsets that display inflammatory markers including CXCR3, CXCR4, and IL-21R as well as elevated levels of CD19 occurred. Of

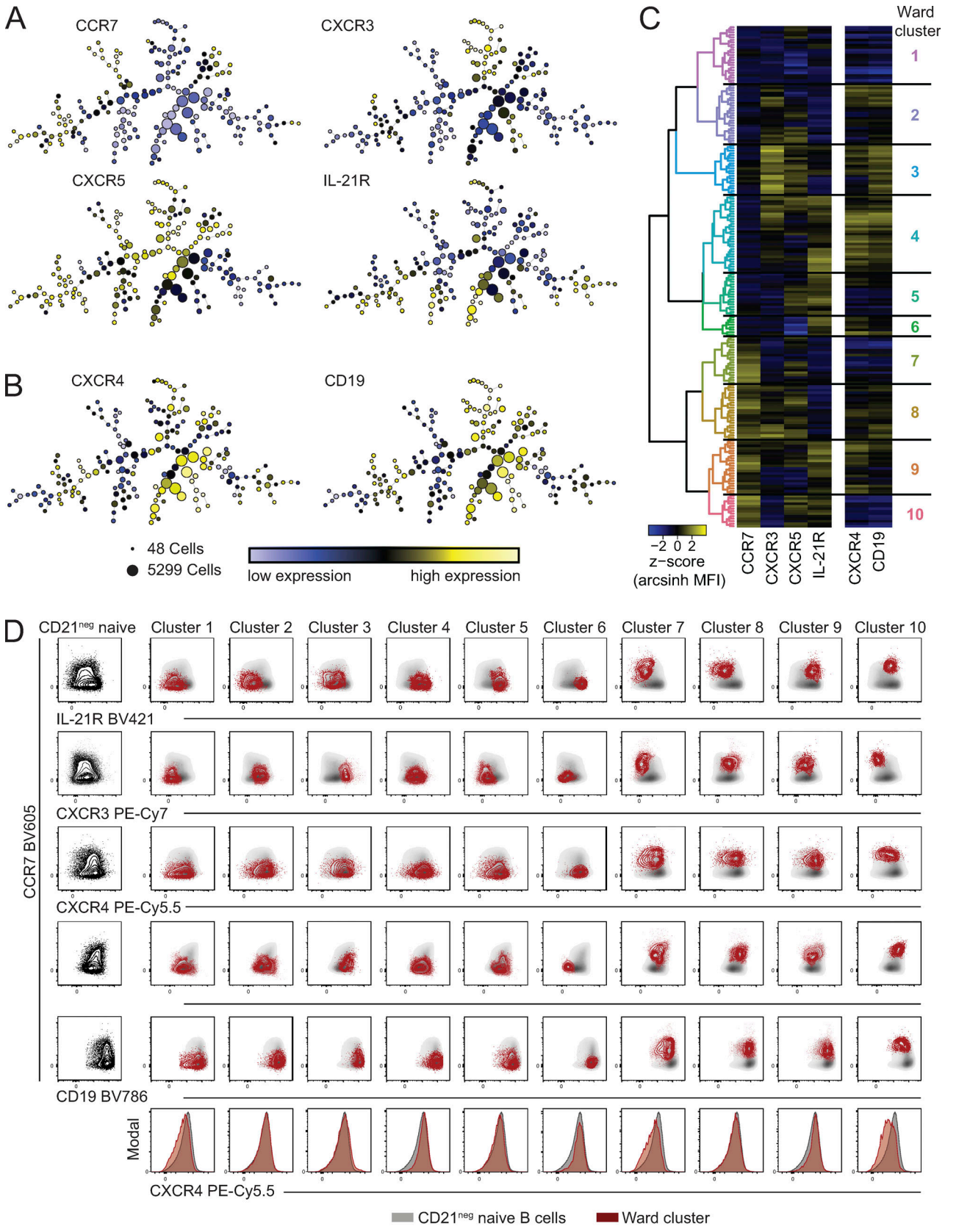

Figure 6. **Computational clustering algorithm SPADE reveals heterogeneity of CD21^{neg} naive B cells in chronic HIV-1 infection. (A)** SPADE trees from combined CD21^{neg} naive B cells of chronic (*n* = 17, chronic 2 yr) HIV-1–infected patients are shown. Expression levels of markers used for clustering (see Materials and methods) are depicted within dot of each cluster. Dot sizes correspond to cell counts per cluster. **(B)** Expression of CXCR4 and CD19 (not used for clustering) within the SPADE tree. **(C)** Heatmap with expression profile of SPADE clusters ordered using Ward's hierarchical clustering. Similar SPADE clusters

are merged in 10 Ward clusters. Dendrogram is colored according to the cutoff used to define Ward clusters. CD19 and CXCR4 expression profile of each SPADE cluster is shown on the right. **(D)** Flow cytometry analysis of Ward clusters from all combined chronic 2-yr samples (n = 17) used for SPADE/Ward clustering. CD21^{neg} naive B cells (red) are overlaid on total CD21^{neg} B cells (gray). Total CD21^{neg} B cells are shown in the first column. Data represent single measurements from each patient time point assessed.

note, we also observed intriguing interdependencies between phenotypic marker expression and clinical parameters in naive and MZ B cell subsets in chronic HIV-1–infected patients (chronic 2 yr time point). CD21^{pos} naive B cells showed a positive correlation of CD19 levels with both CXCR3 and IL-21R, while CD19 correlated solely with CXCR4 in CD21^{neg} naive B cells (Fig. 7 C). Collectively, the side-by-side comparison of healthy and HIV-1–infected donors validated that the defined Ward clusters represent common naive and MZ B cell subsets and allowed the definition of distinct subsets and markers affected by HIV-1 infection.

CD21^{neg} naive and CD21^{neg} MZ B cells display markers linked with distinct functional properties

Anergic naive B cells compose ≤30% of naive B cells in healthy individuals and increase in autoimmunity and viral diseases (Duty et al., 2009; Rakhmanov et al., 2009; Isnardi et al., 2010; Tipton et al., 2015; Flint et al., 2016). These cells exhibit low IgM levels (Duty et al., 2009; Quách et al., 2011) and reduced expression of CD21 (Rakhmanov et al., 2009; Quách et al., 2011; Tipton et al., 2015). Autoreactivity is enriched in IgM^{low} naive B cells, and reduced responsiveness of autoreactive B cells to antigen-dependent stimulation is likely an important mechanism of peripheral tolerance (Quách et al., 2011). To probe if CD21^{neg} naive and CD21^{neg} MZ B cells share similarities with anergic B cells, we analyzed IgM expression in a subset of chronically HIV-1–infected individuals from the longitudinal cohort (n = 6) and healthy controls (n = 29; Fig. 8, A and B). CD95 and FcRL4 expression was recorded, as elevated expression of these markers defines B cell activation and exhaustion (Moir et al., 2008; Sciaranghella et al., 2013; Portugal et al., 2015). Frequencies of IgM^{low} cells were generally higher in CD21^{neg} compared with CD21^{pos} naive B cells, as described (Quách et al., 2011; Fig. 8 C). However, decreased frequencies of IgM^{low} cells in both subsets were observed in HIV-1 infection (Fig. 8 B), while IgM^{low} frequencies of MZ B cells were unchanged (Fig. 8, B and C). Elevated frequencies of IgM^{low} cells suggest that CD21^{neg} naive B cells indeed comprise a higher proportion of anergic and autoreactive B cells.

In line with an activated state, CD95 and FcRL4 were generally expressed at higher levels on CD21^{neg} subsets (Fig. 8 C). HIV-1 infection led to increased CD95 expression on naive and MZ B cells across CD21 subsets, which was most pronounced in acute infection (Fig. 8 B). The same pattern was observed for FcRL4 expression, with the exception of CD21^{pos} naive B cells, where no alteration in response to HIV-1 infection was evident (Fig. 8 B). Importantly, ART successfully reduced CD95 and FcRL4 to healthy donor levels in all subsets. This mirrored the effects observed for memory B cell subsets (Fig. 8, D and E). Except for IM B cells, CD95 and FcRL4 were elevated and reverted to healthy donor levels upon prolonged ART (Fig. 8, D and E).

Collectively, CD21^{neg} naive and CD21^{neg} MZ B cells showed features of recent activation (Fig. 8). In healthy donors (n = 29), this was accompanied with increased proliferation (Ki-67 expression) compared with the CD21^{pos} subsets (Fig. 9, A and B). Chronic HIV-1 infection (n = 21) increased Ki-67 expression in CD21^{pos} subsets over healthy donor levels comparable to the level in CD21^{neg} subsets (Fig. 9 B).

Increased expression of CD95 suggests that CD21^{neg} naive and CD21^{neg} MZ B cells may be sensitive to extrinsic proapoptotic signals. We therefore investigated ex vivo whether these cells are apoptotic. Higher frequencies of cleaved caspase 3^{pos} Annexin V^{pos} apoptotic cells were observed in CD21^{neg} naive and CD21^{neg} MZ B cells of healthy (n = 10) and chronically HIV-1–infected (n = 10) individuals (Fig. 9, C and D). Notably, CD21^{neg} naive B cells from HIV-1–infected people had more apoptotic cells than in healthy donors, emphasizing that chronic HIV-1 infection drives apoptosis in naive B cells. We conclude that CD21^{neg} subsets of naive and MZ B cells reflect a general state of activation, proliferation, and exhaustion at the investigated time point. CD21^{neg} naive B cells in particular include phenotypes linked with anergic, autoreactive, and apoptotic cells.

Reduced responsiveness of CD21^{neg} naive and CD21^{neg} MZ B cells

To probe if CD21^{neg} naive and CD21^{neg} MZ B cells are indeed anergic, we next tested their potential to respond to BCR-dependent stimulation. We applied Phosflow (Schulz et al., 2012) to measure tyrosine phosphorylation in untreated or anti-IgA/-IgM/-IgG stimulated naive and MZ B cells. Memory B cell subsets (IM, RM, AM, and TLM) were analyzed in comparison (Fig. 10, A–D). RM cells, known to be in a quiescent state, had the highest potential to respond to stimulation, while the exhausted TLM cells were the least responsive to BCR cross-linking (Fig. 10, B–D). Of note, basal phosphorylation levels were highest in AM cells, in line with a recent stimulation in vivo (Fig. 10, B–D).

CD21^{neg} MZ B cells of healthy individuals (n = 10) and CD21^{neg} naive and CD21^{neg} MZ B cells of HIV-1–infected individuals (n = 10) showed increased basal phosphorylation over the corresponding CD21^{pos} subsets (Fig. 10 C). This indicates that CD21^{neg} naive and CD21^{neg} MZ B cells had undergone recent activation-induced phosphorylation. Reactivity to BCR stimulation was lower in CD21^{neg} naive B cells compared with CD21^{pos} naive B cells, suggesting that these cells had reached an anergic state (Fig. 10, C and D). Based on absolute expression levels (mean fluorescence intensity [MFI]), CD21^{neg} and CD21^{pos} MZ B cells showed an identical capacity to react to BCR triggering in healthy donors, but the response of CD21^{neg} MZ B was reduced in HIV-1 infection (Fig. 10 C). However, considering fold difference between basal phosphorylation levels and levels upon

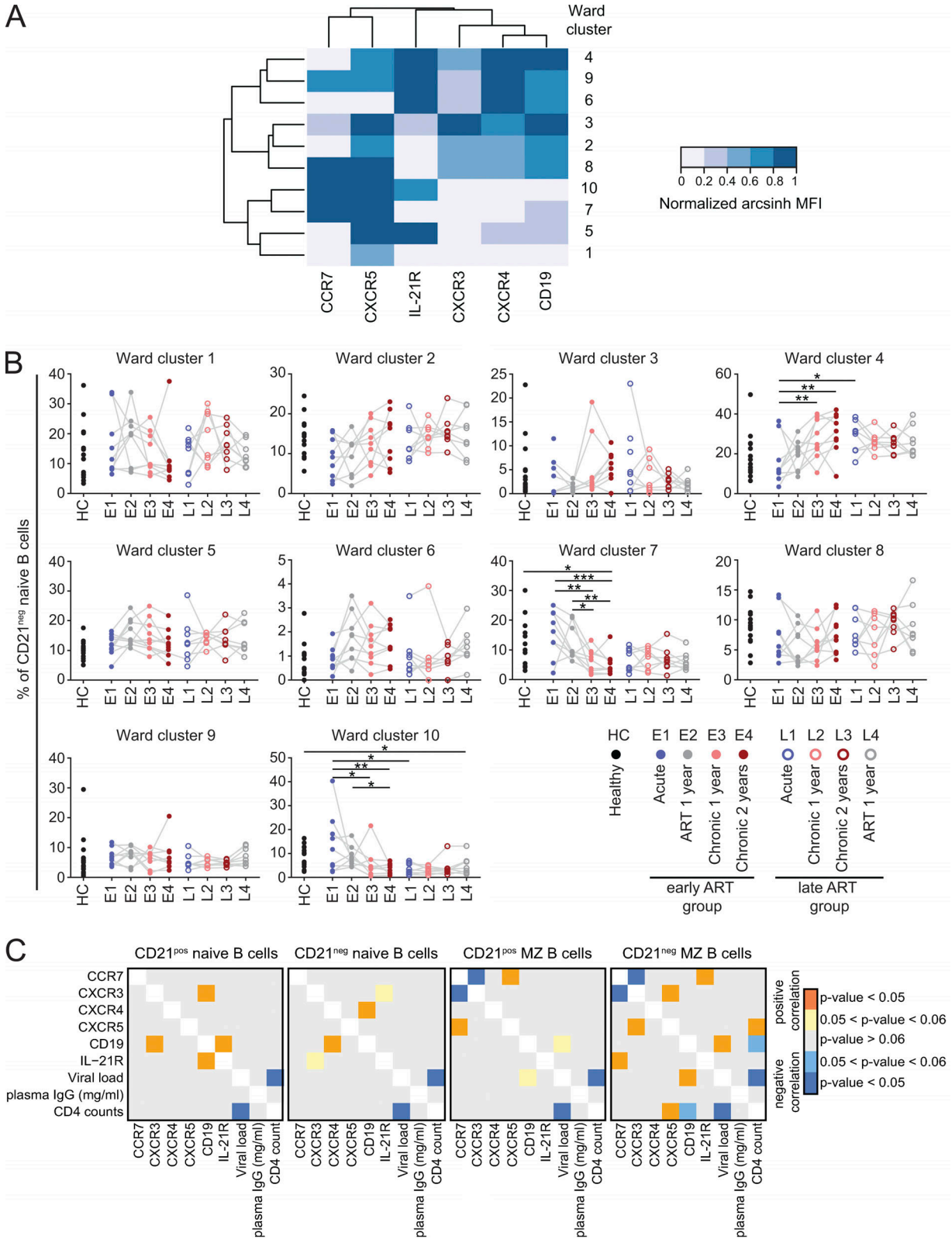

Figure 7. **Longitudinal ward cluster dynamics in HIV-1 infection. (A)** Expression levels of CCR7, CXCR3, CXCR4, CXCR5, IL-21R, and CD19 on Ward clusters from HIV-1–infected patients (n = 17; chronic 2 yr) are shown as z-score of arcsinh-transformed MFI values normalized between 0 and 1 (see Materials and methods). **(B)** Comparison of Ward cluster frequencies between healthy donors (black dots, n = 15) and acute (blue), chronic 1 yr (light red), chronic 2 yr (dark red), and ART 1 yr (gray) time point of HIV-1–infected patients, which were separated into early (closed dots, n = 9) and late (open circles, n = 8) ART initiation groups. P values were derived from linear mixed-effect models with Tukey's method for multiple comparison (see Materials and methods). *, P < 0.05; **, P < 0.01; ***, P < 0.001. **(C)** Spearman correlation of expression of CCR7, CXCR3, CXCR4, CXCR5, and IL-21R in addition to log-transformed viral load, plasma IgG

levels (mg/ml), and CD4 counts from HIV-1–infected individuals (chronic 2 yr; see also Table S2) for CD21^{neg} and CD21^{pos} naive and CD21^{neg} and CD21^{pos} MZ B cells. P values from Spearman correlation were considered significant when P < 0.05 and are colored orange for positive and dark blue for negative correlation. P values between 0.05 and 0.06 are colored yellow for positive and light blue for negative correlation and highlight trends. Nonsignificant values are shown in gray. Data represent single measurements from each patient time point assessed.

stimulation instead of MFI revealed that a lower reactivity of CD21^{neg} MZ B cells was also prevalent among healthy donors (Fig. 10 D).

Overall, we observed an impaired stimulation potential in memory B cell subsets and MZ B cells with an activated phenotype (AM, TLM, and CD21^{neg} MZ B cells) but not in resting cells (RM, IM, and CD21^{pos} MZ B cells) in HIV-1 infection (Fig. 10 E). The notable exception was the CD21^{neg} naive B cell subset, which showed overall reduced responsiveness that was not influenced by HIV-1 infection (Fig. 10 E).

Discussion

Alterations of the B cell compartment induced by HIV-1 infection are characterized by increased levels of transitional B cells and plasmablasts and skewing of memory B cells toward activated and exhausted phenotypes (Moir et al., 2008, 2010; Moir and Fauci, 2013). Whether these perturbations extend to other B cell subsets has not been systematically investigated. Using high-dimensional flow cytometry, we define here B cell signatures associated with progressing HIV-1 infection that reveal a severe impact on naive and MZ B cells.

Increased frequencies of CD21^{neg} memory B cells are a hallmark of HIV-1 infection (Moir et al., 2008, 2010). Here we report that a substantial proportion of naive and MZ B cells also lack CD21 in chronic HIV-1 infection (Fig. 1 D). Intriguingly, CD21^{neg} cells constitute only a minor fraction of naive B cells in healthy individuals, but increased frequencies are described in common variable immunodeficiency and autoimmune disorders (Rakhmanov et al., 2009; Isnardi et al., 2010; Tipton et al., 2015; Flint et al., 2016). These cells express high levels of activation markers such as CD95 and exhibit impaired response to activation in vitro (Rakhmanov et al., 2009; Isnardi et al., 2010). As we demonstrate here, CD21^{neg} naive B cells in HIV-1 infection show high similarities with CD21^{neg} naive B cells described in autoimmune diseases. Resolving the origin and fate of these cells, whether they evolve from classical CD21^{pos} naive B cells upon activation or have individual development paths, will be of interest in HIV-1 infection and beyond.

Aberrant MZ B cell responses associated with a CD21^{neg} phenotype as we describe have not been intensively studied (Terrier et al., 2011). Our detailed phenotypic analyses provide important insights into the properties of CD21^{neg} MZ B cells, which we found share many features with CD21^{neg} subsets of naive and memory B cells. The strong association of CD21^{neg} MZ B cells with CD4 counts and viral load in chronic HIV-1 infection suggests that their activation and exhaustion state is linked with virus-induced immune activation (Fig. 2). In contrast, CD21^{neg} naive B cells are not associated with these clinical factors, suggesting that this subset is steered by other factors during HIV-1 infection. Our findings highlight the need for a systematic investigation of the triggers that lead to CD21^{neg} MZ and CD21^{neg} naive B cell emergence and their consequence for consecutive immune responses.

MZ B cells are involved in IgM responses and, owing to their low potential to undergo class-switch recombination, likely play a minor role in IgG responses (Kruetzmann et al., 2003; Seifert et al., 2015). In line with this, we found HIV-1–specific IgG1 responses to correlate with CD21^{neg} naive but not CD21^{neg} MZ B cells. CD21^{neg} naive B cells were linked with HIV-1–specific IgG1 responses, particularly in the acute phase, and thus may impact de novo responses to HIV-1. Persistent antigen exposure in chronic HIV-1 infection drives the expansion of large clonal families of B cells (Liao et al., 2013; Doria-Rose et al., 2014), which may constrict the impact on the de novo responses and dependence on naive B cells. Delineating the contribution of CD21^{neg} naive B cells in the HIV-1–specific antibody response in forthcoming studies will be of importance to understand their role in shaping antibody responses to HIV-1 at different disease stages.

HIV-1 infection is associated with impaired antibody responses against other pathogens and vaccines (Titanji et al., 2006; Fritz et al., 2010; Kernéis et al., 2014). IgM responses to vaccination appear to be more severely impaired by progressed HIV-1 infection compared with IgG (Fritz et al., 2010). This suggests that de novo induction of IgM by naive B cells, but not reactivation of IgG from memory B cells, is affected (Fritz et al., 2010; Pape et al., 2011). As we show here, a large pool of naive B cells in HIV-1 infection is anergic, which may be a main cause of the impaired antibody responses (Fig. 10, A–C).

Immune responses against bacterial polysaccharides are largely dependent on MZ B cells, and splenectomy has been linked with higher risk of infections with bacterial pathogens such as *Streptococcus pneumoniae* (Kruetzmann et al., 2003; Weill et al., 2009). Infections associated with dramatic alterations of the B cell compartment, such as HIV-1, show reduced responses against polysaccharide-based vaccines and are associated with increased risk of bacterial coinfections. However, the reasons for this defect have thus far been unclear (Zhang et al., 2015; Sadlier et al., 2016). The extensive emergence of nonresponsive CD21^{neg} MZ B cells that we document here provides a plausible cause for the impaired responses.

The dysfunction of CD4 T cells induced by HIV-1 severely impacts B cell responses (Day et al., 2006; Walker and McMichael, 2012). CD4 follicular helper T (T_{FH}) cells are impaired in their ability to provide B cell help (Cubas and Perreau, 2014). Increased levels of PD-L1 on B cells drive dysfunction of T_{FH} cells. Thus, defects of T and B cells directly affect each other, and suboptimal T_{FH} cell help may drive the exhaustion of naive and memory B cells (Cubas et al., 2013). It will thus be important to establish in forthcoming studies whether dysfunctions of the

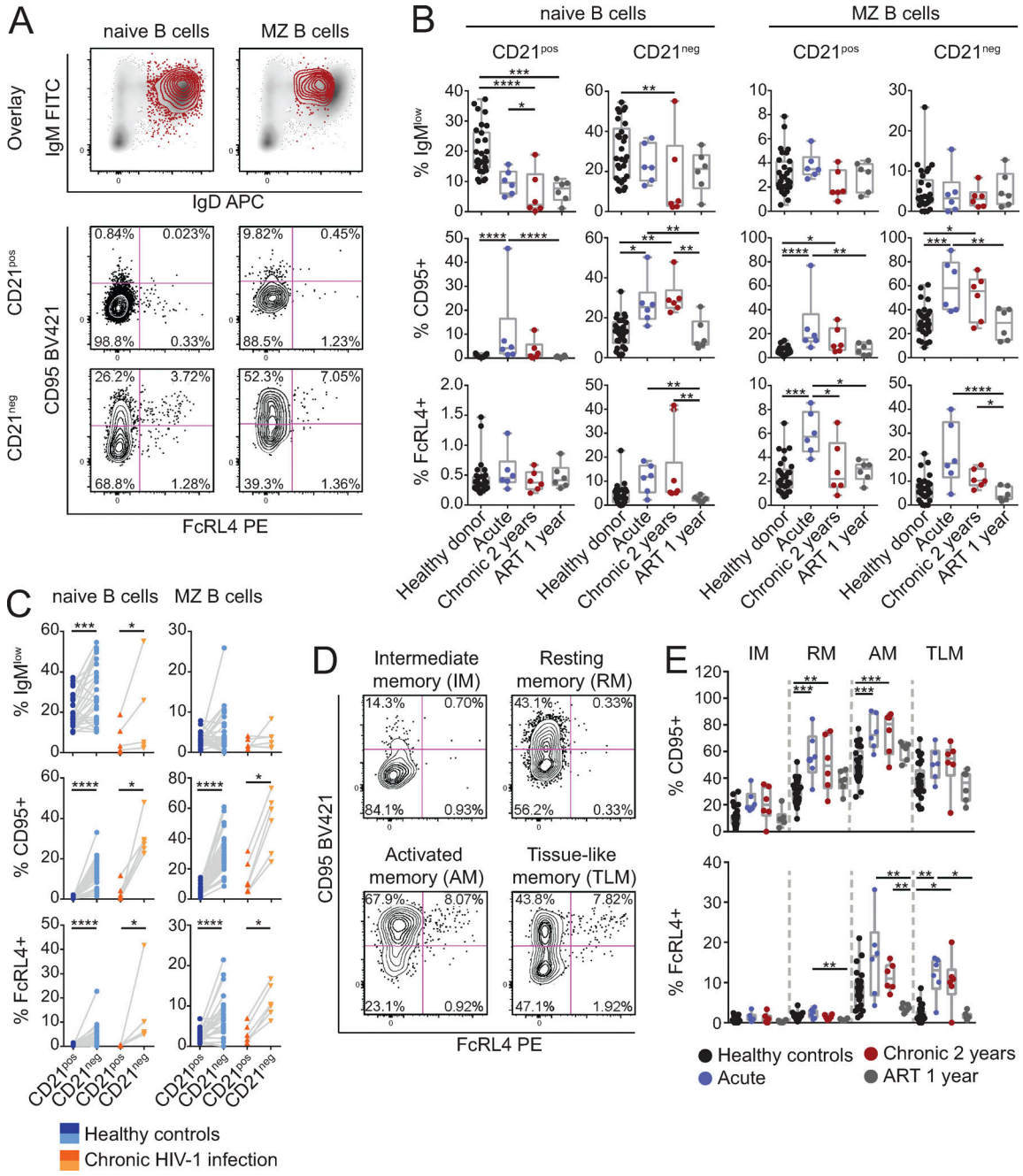

Figure 8. **CD21^{neg} naive and CD21^{neg} MZ B cells are highly activated. (A)** Example of IgM, CD95, and FcRL4 staining for a HIV-1–infected donor (chronic 2 yr). Top row: IgM and IgD expression on CD21^{neg} naive and CD21^{neg} MZ B cells (red) overlaid on total B cells (gray). Bottom rows: CD95 and FcRL4 expression on CD21^{pos} and CD21^{neg} naive and CD21^{pos} and CD21^{neg} MZ B cells. **(B)** IgM, CD95, and FcRL4 expression dynamics of the same subsets from healthy controls (n = 29) and HIV-1–infected patients (n = 6) at acute, chronic 2 yr, and ART 1 yr time points. **(C)** Comparison of IgM, CD95, and FcRL4 expression on B cell subsets in healthy subjects (n = 29) and chronic HIV-1–infected patients (n = 6). Comparison between CD21^{neg} and CD21^{pos} naive and CD21^{neg} and CD21^{pos} MZ B cells within the same individual was done using Wilcoxon signed rank test. **(D)** Flow cytometry dot plots of CD95 and FcRL4 expression on IM, RM, AM, and TLM B cells for HIV-1–infected patient (chronic 2 yr). **(E)** Comparison of CD95 and FcRL4 expression on memory B cell subsets. Analysis was performed on healthy controls (n = 29) and different time points of HIV-1–infected patients (n = 6). P values in B and E were derived from linear mixed-effect models with Tukey's method for multiple comparison (see Materials and methods). P < 0.05 was considered statistically significant. *, P < 0.05; **, P < 0.01; ***, P < 0.001; ****, P < 0.0001. Data represent single measurements from each patient time point assessed. Numbers in dot plots in A and D indicate percentage of gated population. Error bars in B and E depict minimum to maximum range.

T cell compartment drive the emergence of CD21^{neg} naive and CD21^{neg} MZ B cells during HIV-1 infection.

Interestingly, poly- and autoreactive BCRs are enriched within CD21^{neg} B cells in healthy individuals and autoimmune diseases (Isnardi et al., 2010; Saadoun et al., 2013). Their pronounced phenotypic similarity with B cells in autoimmunity raises the possibility that CD21^{neg} naive B cells in HIV-1 may also be enriched for polyreactivity. Investigations of large patient

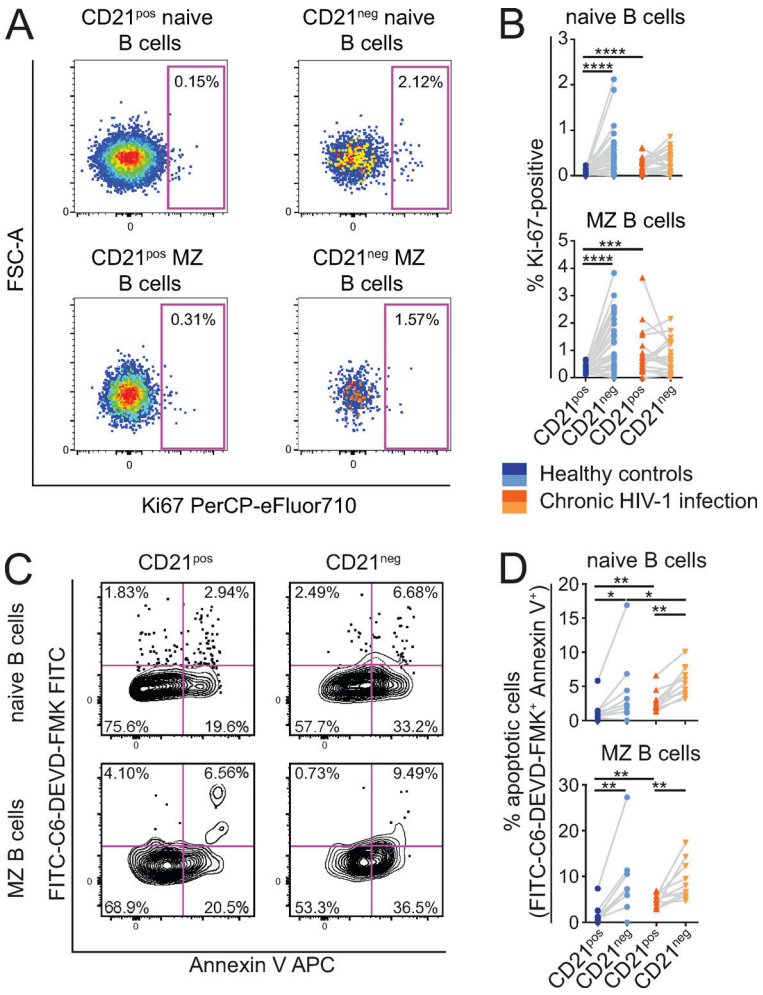

Figure 9. **CD21^{neg} naive and CD21^{neg} MZ B cells are in a proliferative state and are prone to apoptosis. (A)** Example staining for a healthy donor. FSC-A, forward scatter area signal. **(B)** Comparison of Ki-67 expression in B cell subsets in healthy controls (n = 29) and chronic HIV-1–infected patients (n = 21). **(C)** Dot plots of FITC-labeled caspase-3 inhibitor FITC-C6-DEVD-FMK and Annexin V staining from a chronic HIV-1–infected patient. **(D)** Frequencies of apoptotic CD21^{neg} and CD21^{pos} naive and MZ B cells in healthy controls (n = 10) and a set of chronic HIV-1–infected patients (n = 10), where double-positive events in C are defined as apoptotic. Data represent single measurements from each patient time point assessed. Comparison between CD21^{neg} and CD21^{pos} naive and CD21^{neg} and CD21^{pos} MZ B cells within the same individual was done using Wilcoxon signed rank test and between healthy and HIV-1–infected individuals using Mann–Whitney U test. *, P < 0.05; **, P < 0.01; ***, P < 0.001; ****, P < 0.0001. Numbers in dot plots in A and C indicate percentage of gated population.

cohorts will be needed to establish if polyreactivity is indeed common among CD21^{neg} naive B cells and if this is the underlying cause of the emergence of autoantibodies in HIV-1 infection (Shirai et al., 1992; Moir and Fauci, 2009).

Poly- and/or autoreactivity is a common feature of many neutralizing antibodies and bnAbs in HIV-1 infection and contributes to their neutralization activity (Haynes et al., 2005; Mouquet et al., 2010; Liu et al., 2015). Elicitation of polyreactive bnAbs requires a concerted action to overcome immune tolerance mechanisms and may thus be rare (Verkoczy et al., 2010, 2011; Zhang et al., 2016). Autoreactive CD21^{neg} naive and CD21^{neg} MZ B cells could be envisaged to play a role in the elicitation of potent HIV-1–specific bnAbs. Deciphering their role in bnAb induction will be important to potentially harness these cells for vaccine induction of bnAbs.

A large fraction of plasmablasts and IgM^{pos} memory B cells in the periphery of systemic lupus erythematosus (SLE) patients derive from activated naive B cells with similar features as the CD21^{neg} naive B cells described herein (Tipton et al., 2015). These activated naive B cells in SLE showed increased polyreactivity, a remarkable frequency of somatic hypermutation, and the ability to expand resulting in large clonal families. Whether these cells participate in germinal center reaction or are engaged in extrafollicular pathways still need to be resolved, but available data highlight that activated CD21^{neg} naive B cells can undergo BCR affinity maturation and develop into large clusters of antibody-secreting effector cells in SLE. To explore this potential pathway in HIV-1 infection, dedicated studies are needed to dissect whether CD21^{neg} naive B cells in HIV-1 infection have analogous capacities. The severe exhaustion and anergic state of these cells in HIV-1 infection, however, may be a limitation that needs to be understood to resurrect the functional properties of this cell population.

Combining high-dimensional flow cytometry with unsupervised clustering analysis allowed us to elucidate the phenotypic diversity within CD21^{neg} naive B cells. The analysis revealed 10 phenotypically distinct CD21^{neg} naive B cell clusters in healthy and HIV-1–infected individuals (Figs. 6 and 7). Chronic HIV-1 infection was associated with shifts of these clusters toward phenotypes associated with an inflammatory profile such as increased expression of CXCR3 and reduced levels of CCR7 and CXCR5, which suggests ongoing B cell changes during disease progression. Interestingly, prolonged ART did not revert these phenotypic changes acquired during disease progression in the late ART initiation group (Figs. 5 and 7 B). Of note, exhausted T cells do not revert their phenotype upon antigen withdrawal or immunotherapy with checkpoint inhibitors, since the exhaustion phenotype characterized by high expression of PD-1 is

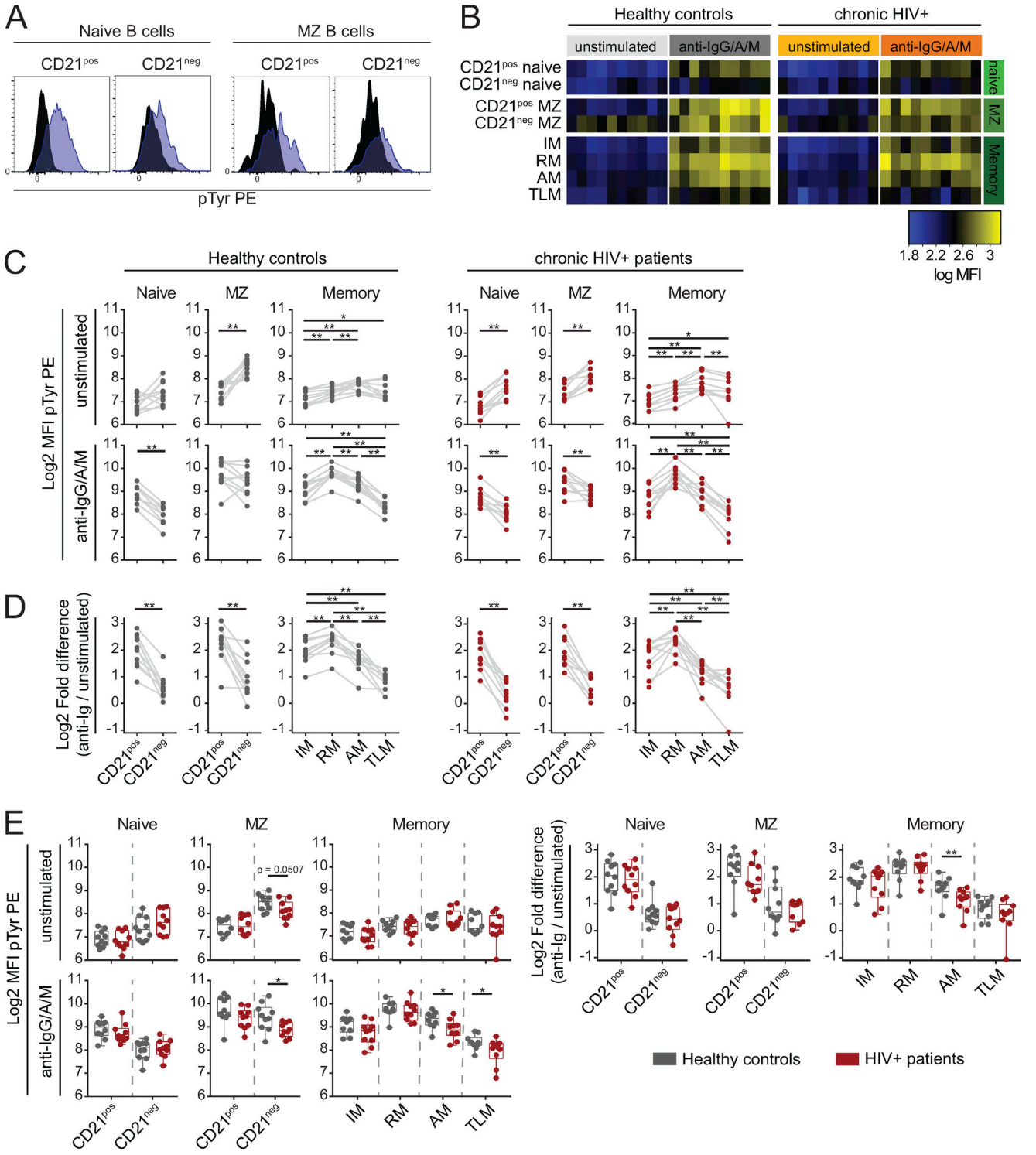

Figure 10. **CD21^{neg} naive and CD21^{neg} MZ B cells are in an anergic state. (A)** Histogram overlays of flow cytometric Phosflow analysis in unstimulated (black) and BCR cross-linking stimulated (blue) CD21^{neg} and CD21^{pos} naive and CD21^{neg} and CD21^{pos} MZ B cells from a chronic HIV-1–infected patient. **(B)** Tyrosine phosphorylation (log-transformed MFI values) before and upon stimulation with anti-IgG/IgA/IgM in healthy subjects (n = 10) and chronic HIV-1–infected patients (n = 10) for CD21^{neg} and CD21^{pos} naive B cells, CD21^{neg} and CD21^{pos} MZ B cells, and IM, RM, AM, and TLM B cells. **(C and D)** Total log2-transformed tyrosine phosphorylation MFI at basal levels and upon stimulation (C) and log2-transformed fold difference between unstimulated and IgG/IgA/IgM-stimulated CD21^{neg} naive and CD21^{neg} MZ B cells (D) in comparison to their CD21^{pos} counterpart from the same donors shown in B. Memory B cell subsets are included as a control. **(E)** Direct comparison of the above parameters from CD21^{neg} and CD21^{pos} naive B cells, CD21^{neg} and CD21^{pos} MZ B cells, and memory B cell subsets upon stimulation between healthy controls (n = 10) and chronic HIV-1–infected patients (n = 10). Data represent single measurements from each patient time point assessed. Wilcoxon signed rank test was used to compare CD21^{neg} and CD21^{pos} naive and CD21^{neg} and CD21^{pos} MZ B cells within healthy subjects and chronic HIV-1–infected patients. For the comparison between memory B cell subsets, Wilcoxon singed rank test was used. To compare phosphorylation levels between healthy subjects and chronic HIV-1–infected patients, Mann–Whitney U test was applied. P < 0.05 was considered statistically significant. *, P < 0.05; **, P < 0.01. Error bars depict minimum to maximum range.

imprinted in the epigenetic landscape (Utzschneider et al., 2013; Pauken et al., 2016). It will be interesting to explore if analogous effects occur in the B cell compartment in HIV-1 infection. An exception in the response pattern to ART was CD95, expression of which decreased upon treatment (Fig. 8 B). Of note, the activation marker CD95 is decoupled from exhaustion and decreases upon antigen withdrawal such as during successful ART, while the functional and phenotypic characteristics of exhaustion can persist (Sciaranghella et al., 2013).

In summary, our comprehensive longitudinal analysis of the B cell compartment in HIV-1 infection revealed phenotypic signatures associated with chronic immune activation. In particular, we document the emergence of unique CD21^{neg} naive B cell subsets in HIV-1 infection. Dissection of their potential functional differences and developmental pathways will be important future avenues of research to understand the role of CD21^{neg} naive B cells in health and disease. The emergence of anergic naive and MZ B cells we unveil and their phenotypic definition by down-regulation of CD21 and changed chemokine receptor and IL-21R expression patterns will empower future studies to define and trace these cell populations and uncover their functions. The impact of CD21^{neg} naive and CD21^{neg} MZ B cells on the IgA, IgM, and IgG antibody response against coinfections or vaccines in HIV-1–infected patients will be key to resolve. This will be particularly critical in understanding pathogenic changes of the immune system in HIV-1 infection and will accordingly tailor preventive and therapeutic vaccine approaches. Monitoring of these cell populations may be exploited as biomarkers to predict the efficacy of vaccines and of antibody responses against coinfections. Therapeutic interventions with the aim to restore impaired CD21^{neg} naive and CD21^{neg} MZ B cells could improve antibody responses in HIV-1 infection. The knowledge of the phenotypic characteristics of CD21^{neg} naive and CD21^{neg} MZ B cells in HIV-1 infection that our study provides will be vital to all these endeavors.

Materials and methods

Clinical specimens and study approval

Cryopreserved peripheral blood mononuclear cells (PBMCs) and plasma of HIV-1–infected individuals were available from samples stored in the biobank of the ZPHI. The ZPHI is an ongoing, observational, nonrandomized, single-center cohort founded in 2002 that specifically enrolls patients with documented acute (i.e., first 3 mo after infection) or recent (i.e., 3–6 mo after infection) primary HIV-1 infection (ClinicalTrials.gov identifier NCT00537966; Rieder et al., 2011). The ZPHI is approved by the ethics committee of the Kantonale Ethikkommission Zürich, and written informed consent was obtained from all participants. The patient samples analyzed in the current study are derived biobanked samples from two different treatment arms from a historic study assessed as part of the ZPHI from 2002 to 2007 (Gianella et al., 2011; Wyl et al., 2011). One treatment arm (early ART initiation group) started ART during acute infection, stayed on ART for ≥1 yr after suppressed viremia, and then underwent ART interruption. The second treatment arm (late ART initiation group) delayed initiation of ART until the chronic disease stage. Importantly, all patients enrolled in the ZPHI were recommended by the treating physician to initiate early ART.

Patients who opted for early treatment could choose to stay or to interrupt ART after being virologically suppressed ≥1 yr, and reinitiation of ART was performed according to treatment guidelines at that time of study (Hammer et al., 2006). The remaining patients opted to delay or interrupt ART at certain stages, providing the source of the samples studied here.

Longitudinal samples of patients that started ART early (during the acute infection stage, $n = 11$) and late (in the chronic infection stage, $n = 10$) were analyzed and included samples from the untreated acute and chronic stage and after 1 yr of ART (Fig. 1 A; and Tables S1 and S2). For the early ART initiation group, the 1- and 2-yr chronic infection time points were calculated from the time point of ART cessation to guarantee comparable continuous viral replication in both groups.

Patients from both arms were included in our analysis for whom cryopreserved PBMC samples were available at all time points considered in our analysis (acute infection, chronic infection, and prolonged ART). No other selection criteria were applied. A separate set of 10 patients were analyzed during the chronic infection stage for functional analysis of B cell subsets (Figs. 9, C and D; Fig. 10; and Table S2). Patient and disease demographics (estimated time of infection, CD4 T cell count and plasma viral load at sampling date, age, gender, ethnicity, and virus subtype) were available through the ZPHI database (Table S2). PBMCs and plasma from healthy, HIV-1–uninfected donors ($n = 29$) were collected in the frame of a separate clinical study (principal investigator, H. Günthard) that was approved by the ethics committee of the Kantonale Ethikkommission Zürich, and written informed consent was obtained from all participants.

PBMCs were isolated by density-gradient centrifugation using LymphoPrep (Axis-Shield) from whole blood drawn in EDTA vacutainer tubes (BD Biosciences). Until further processing, PBMCs were cryopreserved using 90% inactivated FCS (Thermo Fisher Scientific) and 10% DMSO (Sigma-Aldrich) and stored in liquid nitrogen. Plasma was heat-inactivated for 1 h at 56°C and stored at −80°C.

Flow cytometry

To monitor B cell populations by flow cytometry, PBMCs were stained using an 18-parameter panel as described in detail in Liechti et al. (2018a). Briefly, cells were thawed and washed with FACS buffer containing PBS (Thermo Fisher Scientific), 2% heat-inactivated FCS (Thermo Fisher Scientific), 2 mM EDTA (Sigma-Aldrich), and 20 µg/ml DNase (Sigma-Aldrich) and stained with live/dead fixable near-infrared dye (Life Technologies) for 30 min, enabling dead cell exclusion. Viability staining was followed by a surface staining step with antibodies directed against CCR7 BV605 (G043H7; BioLegend), CD3 APC-Cy7 (SK7; BioLegend), CD10 BV650 (HI10a; BD Biosciences), CD14 APC-Cy7 (HCD14; BioLegend), CD16 APC-Cy7 (3G8; BioLegend), CD19 BV786 (SC25C1; BD Biosciences), CD21 BV711 (B-ly4; BD Biosciences), CD27 PE-CF594 (M-T271; BD Biosciences), CD38 Alexa Fluor 700 (HIT2; BioLegend), CXCR3 PE-Cy7 (G025H7; BioLegend), IL-21R BV421 (2G1-K12; BioLegend), CXCR5 BV510 (RF8B2; BD Biosciences), IgA APC (polyclonal goat IgG; Jackson

ImmunoResearch), IgG1 PE (HP6001; Southern Biotech), and IgG3 FITC (polyclonal sheep IgG; AbD Serotec). Unlabeled CXCR4 (12G5; BioLegend) and IgD (IA6-2; BioLegend) were conjugated in-house with PE-Cy5.5 and PE-Cy5, respectively, using the Lightning-Link conjugation kits from Innova Biosciences according to the manufacturer's instructions. Cells were then fixed and permeabilized with the FoxP3/Transcription factor staining kit (eBioscience) according to the manufacturer's instructions to stain for Ki-67 PerCP-eFluor710 (clone 20Raj1; eBioscience).

Data were acquired on a BD Fortessa calibrated daily using the BD Bioscences Cytometer Setup and Tracking module. Staining intensity quality control was conducted as recommended (Roederer et al., 2015), and individual stainings with markers that did not fulfil requirements were excluded when comparative analysis of intensities was performed (Fig. S1 C). To further limit the possibility of influence from day-to-day variability in the flow cytometry analysis, all longitudinal time points of a given patient were run on the same day. In addition, patients assigned to the early and late ART groups were included in all experiments to exclude batch effects. Antibodies and reagents used to analyze IgM, CD95, and FcRL4 expression included CD10 BV650 (HI10a; BD Biosciences), CD19 BV510 (SJ25C1; BD Biosciences), CD21 BV711 (B-ly4; BD Biosciences), CD7 PE-CF594 (M-T271; BD Biosciences), CD38 Alexa Fluor 700 (HIT2; BioLegend), CD95 BV421 (DX2; BioLegend), FcRL4 PE (413D12; BioLegend), IgD APC (IA6-2; BioLegend), IgG PE-Cy7 (G18-145; BD Biosciences), IgM FITC (polyclonal goat IgG; Caltag), and live/dead near-infrared dye (Life Technologies). On some occasions, fluorescence minus one (FMO) controls containing all antibodies except the one of interest were used to determine negative and positive cells, which is particularly useful for dim markers.

Clustering analysis

The diversity of CD21^{neg} naive B cells was assessed using the clustering algorithm SPADE integrated into the cytometry analysis platform Cytobank (Chen and Kotecha, 2014). SPADE allows clustering of cells based on similar expression pattern of markers and visualizes clusters in minimum spanning tree structures (Qiu et al., 2011). 17 of the 21 HIV-1–infected patients were included in the clustering analysis. Two patients had to be excluded because no sample from the acute time point was available, and two were excluded due to low staining of IL-21R and CXCR5 due to technical variation, as depicted in Fig. S1 C. As a reference, 15 healthy controls were included in the analysis.

Clustering was done using pregated CD21^{neg} naive B cells including all recorded events. The target number of expected nodes was set to 200 and down-sampling to 2%. To analyze total longitudinal changes of CD21^{neg} naive B cells, the flow cytometry files of the individual time points or the control group were concatenated and integrated into the clustering. Clustering was based on the markers CCR7, CXCR3, CXCR5, and IL-21R. The four parameters chosen for clustering were characterized by bimodal expression patterns, a requirement for best possible cluster allocation. CD19 was not selected for clustering due to its unimodal expression profile. CXCR4 was not selected for clustering due to variability in staining intensity (Fig. S1 C). The generated SPADE trees showed a clear allocation of cells in clusters with specific expression patterns (Fig. 6 A). We chose a setting of overclustering, by allowing for 200 different clusters, as this allows one to build separate clusters of very rare cell populations. As a consequence, frequent cell populations can separate into different clusters despite sharing phenotypic properties. Therefore, clusters created by SPADE were further clustered using hierarchical clustering with the Ward method Ward.D2 in R and visualized with the heatmap.2 function. For Ward clustering and visualization, the SPADE output (z-transformed arcsinh median fluorescence intensities of individual clusters) of the concatenated chronic 2-yr samples was used due to the fact that this measurement encompassed the highest frequency of CD21^{neg} naive B cells, and therefore all SPADE clusters should contain cell events. We excluded SPADE cluster 200, which showed unusually low CXCR5 levels below background noise. Importantly, we based the Ward clustering on the same markers used for SPADE clustering. CXCR4 and CD19 expression of the SPADE clusters was visualized to investigate the expression profile of these two markers on SPADE and Ward clusters. Based on the Ward hierarchical tree, we merged the 200 SPADE clusters into 10 Ward clusters. The arcsinh-transformed MFI values of the 10 Ward clusters were normalized between 0 and 1, with MFI values below the 1st and above the 99th percentile set to 0 and 1, respectively. These values were displayed as a heatmap and colored with increments of 0.2 to depict the expression levels of the individual Ward clusters (Fig. 7 A). Ward clusters and markers in Fig. 7 A were clustered using complete linkage method with Euclidean distance measure. The classification was confirmed by manually inspecting expression profiles of Ward clusters (Fig. 6 D). For manual analysis, the SPADE clusters of the concatenated chronic 2-yr samples were again concatenated according to the Ward cluster classification. The cell events of these Ward clusters were further analyzed in FlowJo version 10 (TreeStar) to assess the unique expression profile of the Ward clusters.

IgG ELISA

Total IgG concentrations in heat-inactivated plasma from the HIV-1–infected patients (Table S2) were measured by ELISA as described previously (Trkola et al., 2004). Briefly, 96-well immunosorbent plates (Thermo Fisher Scientific) were coated with polyclonal goat anti-human IgG (2 µg/ml; Southern Biotech) in sodium carbonate buffer, pH 8.2, for 2 h at room temperature. PBS/2% BSA (Sigma-Aldrich) was used as a blocking reagent for 30 min at 37°C. Serial dilutions of the plasma samples were applied to the plates and incubated for 2 h at room temperature. Plasma IgG was detected using a biotinylated polyclonal goat anti-human IgG (Southern Biotech; 2 ng/ml) followed by streptavidin-alkaline phosphatase (Sigma-Aldrich; 40 ng/ml), each diluted in PBS/2% BSA and incubated for 1 h at room temperature. CDP-Star System (Applied Biosystems) was used as alkaline phosphatase substrate, and luminescence was measured after 30 min with a Dynex luminometer (Magellan Biosciences). Human IgG (Sigma-Aldrich) was used as a standard to determine the concentration of plasma IgG.

Expression of apoptosis markers

To determine the frequency of apoptotic cells, we analyzed two major events during apoptosis using flow cytometry: cleavage of caspase 3 and the exposure of phosphatidylserine on the outer leaflet of the cell membrane (Segawa et al., 2014). Cryopreserved PBMCs from 10 healthy controls and 10 chronically infected patients were analyzed for the frequency of apoptotic cells within the different B cell subsets (Table S2). PBMCs were stained for 30 min with antibodies against surface markers including CD19 biotin (HIB19; BD Biosciences), CD21 PE (B-ly4; BD Biosciences), CD27 PE-CF594 (M-T271; BD Biosciences), IgD PE-Cy7 (IA6-2; BioLegend), and the apoptosis markers cleaved caspase 3 inhibitor FITC-C6-DEVD-FMK (AAT Bioquest). Subsequently, live/dead near-infrared dye (Life Technologies) and streptavidin BV421 (BioLegend) staining was performed for 30 min followed by staining with Annexin V APC (BD Biosciences) according to the manufacturer's protocol. Samples were analyzed on either a FACS Aria III or a BD FACS Verse immediately after staining and analyzed with FlowJo version 10. Apoptotic cells were defined as double positive for Annexin V and FITC-C6-DEVD-FMK (Jayaraman, 2003) after dead cell exclusion using live/dead near-infrared dye.

Phosflow analysis

PBMCs were rested after thawing for 4 h in RPMI 1640 medium (Thermo Fisher Scientific) without supplements and subsequently incubated in RPMI 1640 containing live/dead near-infrared dye (Life Technologies) for 20 min at room temperature. Cells were washed, split into two wells, and resuspended in either only RPMI 1640 for the unstimulated sample or RPMI 1640 containing 10 µg/ml goat anti-human IgG/IgA/IgM f(ab) 2 (Jackson ImmunoResearch). Stimulation was done for 5 min including a 2-min centrifugation step to remove the medium, followed by addition of the fixation and permeabilization solution of the Foxp3 staining kit according to the manufacturer's instructions (eBiosciences). Cells were fixed and permeabilized for 45 min at 4°C and then stained with antibodies including CD3 APC-Cy7 (SK7; BioLegend), CD10 PE-Cy5 (HI10a; BD Biosciences), CD14 APC-Cy7 (HCD14; BioLegend), CD16 APC-Cy7 (3G8; BioLegend), CD19 BV510 (SJ25C1; BD Biosciences), CD21 BV711 (B-ly4; BD Biosciences), CD27 PE-CF594 (M-T271; BD Biosciences), IgD APC (IA6-2; BioLegend), and total phosphortyrosine PE (PY20; BD Biosciences) for 30 min at room temperature. Cells were extensively washed and measured using a BD Fortessa. Analysis was done with FlowJo 10 (TreeStar).

Assessment of the HIV-1–binding antibody response in plasma

Plasma IgG1 antibody responses were measured with a customized multiplex immunoassay as described (Kadelka et al., 2018; Liechti et al., 2018b). The assay enables the analysis of IgG subclass responses against antigens derived from HIV-1. Sources of antigens and detailed assay protocols have been described in detail (Kadelka et al., 2018; Liechti et al., 2018b). Antigens included matrix (p17; strain NL4-3) and capsid protein (p24; strain BH10), linear peptides from the variable loop 3 (V3) of strains JR-FL, MN, and BG505 (V3 JR-FL, V3 MN, and V3 BG505), monomeric gp120 (strain JR-FL; gp120 JR-FL), monomeric gp140 (strain BG505; gp140 BG505 monomer), native-like trimer BG505 SOSIP.664 (gp140 BG505 trimer), the trimeric gp41 lacking the membrane-proximal external region (SF162P3, gp41ΔMPER), linear MPER peptides encompassing the epitopes for the bnAbs 2F5 and 4E10 (MN, MPER-2/4) and in addition for 10E8 (MN, MPER-2/4/10). In addition, resurfaced stabilized core 3 (RSC3) protein containing a preserved CD4 binding site (CD4bs) but lacking immunodominant variable loop regions and its mutant RSC3 Δ371I, which does not react with most CD4bs antibodies, were included to delineate CD4bs-specific responses (Wu et al., 2010). To determine the anti-CD4bs response, we subtracted the signal of RSC3 Δ371I from RSC3 (Lynch et al., 2012). Half-maximum titers (EC50) were calculated from dilution series of heat-inactivated plasma with six fivefold dilutions ranging from 1:100 to 1:312,500 using a four-parameter dose–response curve. IgG1 responses are much stronger than IgG2 and IgG3, which is why we only focused on IgG1 responses for Spearman correlations (Fig. S3) to get sufficient signal despite the small sample sizes (acute, $n = 13$; chronic 2 yr, $n = 14$).

Statistical analysis

Statistical analyses were performed in Python 2.7 using the package scipy.stats, in R3.5.1 using its libraries lme4, lmerTest, multcomp, car, and Rtsne, in Prism (GraphPad), as well as with Cytobank (for the SPADE clustering analysis in Fig. 6).

Much data in this paper is of compositional nature (Fig. 1, B–D; Figs. 5 A, 7 B, 8, B and E; and Fig. S2, A–C). That is, the frequencies of various B cell subsets sum up to a value ≤100%. We used a logit transformation (logit in the R package car) to account for this specific type of data. The logit transformation allows more emphasis to be put on differences at both ends of the spectrum [0%,100%] compared with log transformations that put the emphasis solely on the lower end of the spectrum. In Figs. 7 B and 8, B and E, some frequencies are recorded as exactly 0%. In these instances, we first performed a linear transformation of the data from [0,1] into [0.001,0.999] before the logit transformation. For the noncompositional data analyzed in Fig. 5 B, we used a log transformation.

We used a linear mixed-effect model wherever we compared multiple samples from the same HIV-1–infected individuals at different disease stages (Fig. 1, B–D; Figs. 5, 7 B, 8, B and E; and Fig. S2, A–C) to account for the correlation of repeated measurements within patients. Here, the infection stage (healthy, acute, ART, or chronic) constituted the fixed-effect term of the model, while the patient ID constituted the random-effect term. We also assumed that two different subjects have uncorrelated measurements (i.e., the covariance matrix we used was zero off the diagonal): $\text{logit}(Y_{ij}) = \beta_0 + \beta_j X_{ij} + u_i + \varepsilon_{ij}$, where $i = 1, \ldots, |\text{healthy donors}| + |\text{HIV-infected individuals}|$, and $j = 1$ (for healthy donors) or $j = 2, 3, 4$ (for HIV-infected individuals). An F test was performed on the ANOVA table using Satterthwaite's method for the denominator degrees of freedom to check for overall differences. If differences existed ($P < 0.05$), we further used Tukey's method on t test to adjust for the fact that we consider all possible comparisons between disease stages and healthy controls. Unlike log ratio transformation, which is

frequently used in compositional data analysis, this approach allowed us to test if there were differences in each individual B cell subset between the stages (healthy, acute, ART, and chronic), which represents the typical type of analysis in flow cytometry. Furthermore, the approach we chose does not require the stringent assumption of equality of a multivariate covariance matrix.

In Fig. 1 E, we applied the nonlinear dimensionality reduction algorithm tSNE on the z-scores of the frequencies of B cell subsets (shown in Fig. 1, B–D) to obtain a two-dimensional representation of proximity for healthy controls (n = 29) and different time points (acute, chronic 2 yr, and 1 yr of ART) of HIV-1–infected individuals (n = 19 for acute time point, n = 21 for time points chronic 2 yr and 1 yr of ART). To avoid linear dependencies, we excluded the frequencies of total naive, MZ, and memory B cells from the tSNE analysis, since subcategorizations of these B cell subsets were already used as inputs. The distinction of clusters I and II shown as a red dotted line in Fig. 1 E was set manually to characterize clinical features of chronically HIV-1–infected individuals, which overlap with healthy donors. tSNE was run with the Rtsne package in R using the following parameter choices (perplexity, 29; theta, 0; 300,000 iterations).

The Mann–Whitney U test was used to compare the clinical features of clusters I and II in Fig. 1 F, where clusters were defined by the tSNE-mapping shown in Fig. 1 E. Linear regression was used to describe correlations of $CD21^{neg}$ and $CD21^{pos}$ naive and $CD21^{neg}$ and $CD21^{pos}$ MZ B cells with clinical parameters (Fig. 2). Phenotypic comparisons between $CD21^{neg}$ and $CD21^{pos}$ naive or $CD21^{neg}$ and $CD21^{pos}$ MZ B cell subsets within the same patients were done using the Wilcoxon signed rank test (Figs. 3 B; 4 B; 8 C; 9, B and D; and 10, C and D) and between healthy donors and HIV-1–infected patients using the Mann–Whitney U test (Figs. 3 C; 4, B and C; 9, B and D; and 10 E). Spearman correlation was used to calculate the correlation between the indicated markers in Figs. 7 C and S3. All reported statistical analyses are of an explorative, descriptive nature. We therefore opted, by default, not to formally adjust for multiple testing because false positives are less of a problem in explorative studies than false negatives (Saville, 2018). In addition, almost all the associations we focus on exhibit a low P value, much lower than a Bonferroni-corrected P value. Heatmaps and hierarchical clustering were generated in R3.3.1 using the heatmap.2 function.

Online supplemental material

Fig. S1 depicts flow cytometry gating to define B cell subsets using the 16-color flow cytometry staining panel and the signal variation across the entire study for the markers IL-21R, CCR7, CXCR3, CXCR4, CXCR5, Ki-67, and CD19. Fig. S2 shows the comparison of B cell subsets between the early and late ART group. Fig. S3 depicts the Spearman correlation analysis of the binding antibody response against various HIV-1–derived antigens and $CD21^{neg}$ naive and $CD21^{neg}$ MZ B cells and their $CD21^{pos}$ counterpart from acute (n = 13) and chronically (chronic 2 yr, n = 14) infected individuals. Table S1 contains the summarized data of healthy controls and the individual time points of the early and late ART group. Demographic data for each individual and overview of the choice of samples for the individual analyses are listed in Table S2.

Acknowledgments

We thank Annette Oxenius for critical discussions, Bettina Ruehe and Christina Grube for collection of blood from healthy donors, and the Flow Cytometry Facility of the University of Zurich for instrument maintenance. We thank Dr. Philip Dixon and Katie Rey from the Statistics Department at Iowa State University and Dr. Jon Fintzi from the National Institute of Allergy and Infectious Diseases Biostatistics Research Branch at the National Institutes of Health for statistical guidance.

Financial support for this study has been provided by the Swiss National Science Foundation (314730_152663 and 314730_172790 to A. Trkola and 324730B_179571 to H.F. Günthard), the Clinical Priority Research Program of Universität Zürich (Viral infectious diseases: Zurich Primary HIV Infection Study to H.F. Günthard and A. Trkola), the Yvonne-Jacob Foundation (to H.F. Günthard), the Swiss Vaccine Research Institute (to A. Trkola and H.F. Günthard), and the SystemsX.ch grant AntibodyX (to A. Trkola).

The authors declare no competing financial interests.

Author contributions: T. Liechti and A. Trkola conceived and designed the study. T. Liechti performed experiments and data analysis. C. Kadelka and M. Robbiani contributed to data analysis. D.L. Braun, H. Kuster, J. Böni, and H.F. Günthard managed the ZPHI cohort and collected and contributed patient samples and clinical data. T. Liechti, C. Kadelka, M. Robbiani, and A. Trkola wrote the manuscript, on which all coauthors commented.

Submitted: 14 June 2018
Revised: 7 February 2019
Accepted: 24 May 2019

References

Bangs, S.C., A.J. McMichael, and X.N. Xu. 2006. Bystander T cell activation-implications for HIV infection and other diseases. *Trends Immunol.* 27: 518–524. https://doi.org/10.1016/j.it.2006.09.006

Buckner, C.M., S. Moir, J. Ho, W. Wang, J.G. Posada, L. Kardava, E.K. Funk, A.K. Nelson, Y. Li, T.W. Chun, and A.S. Fauci. 2013. Characterization of plasmablasts in the blood of HIV-infected viremic individuals: evidence for nonspecific immune activation. *J. Virol.* 87:5800–5811. https://doi.org/10.1128/JVI.00094-13

Bunnik, E.M., L. Pisas, A.C. van Nuenen, and H. Schuitemaker. 2008. Autologous neutralizing humoral immunity and evolution of the viral envelope in the course of subtype B human immunodeficiency virus type 1 infection. *J. Virol.* 82:7932–7941. https://doi.org/10.1128/JVI.00757-08

Chen, T.J., and N. Kotecha. 2014. Cytobank: providing an analytics platform for community cytometry data analysis and collaboration. *Curr. Top. Microbiol. Immunol.* 377:127–157.

Cubas, R., and M. Perreau. 2014. The dysfunction of T follicular helper cells. *Curr. Opin. HIV AIDS.* 9:485–491. https://doi.org/10.1097/COH.0000000000000095

Cubas, R.A., J.C. Mudd, A.L. Savoye, M. Perreau, J. van Grevenynghe, T. Metcalf, E. Connick, A. Meditz, G.J. Freeman, G. Abesada-Terk Jr., et al. 2013. Inadequate T follicular cell help impairs B cell immunity during HIV infection. *Nat. Med.* 19:494–499. https://doi.org/10.1038/nm.3109

Day, C.L., D.E. Kaufmann, P. Kiepiela, J.A. Brown, E.S. Moodley, S. Reddy, E.W. Mackey, J.D. Miller, A.J. Leslie, C. DePierres, et al. 2006.

PD-1 expression on HIV-specific T cells is associated with T-cell exhaustion and disease progression. *Nature.* 443:350–354. https://doi.org/10.1038/nature05115

Derdeyn, C.A., P.L. Moore, and L. Morris. 2014. Development of broadly neutralizing antibodies from autologous neutralizing antibody responses in HIV infection. *Curr. Opin. HIV AIDS.* 9:210–216. https://doi.org/10.1097/COH.0000000000000057

Diggins, K.E., P.B. Ferrell Jr., and J.M. Irish. 2015. Methods for discovery and characterization of cell subsets in high dimensional mass cytometry data. *Methods.* 82:55–63. https://doi.org/10.1016/j.ymeth.2015.05.008

Doria-Rose, N.A., R.M. Klein, M.G. Daniels, S. O'Dell, M. Nason, A. Lapedes, T. Bhattacharya, S.A. Migueles, R.T. Wyatt, B.T. Korber, et al. 2010. Breadth of human immunodeficiency virus-specific neutralizing activity in sera: clustering analysis and association with clinical variables. *J. Virol.* 84:1631–1636. https://doi.org/10.1128/JVI.01482-09

Doria-Rose, N.A., C.A. Schramm, J. Gorman, P.L. Moore, J.N. Bhiman, B.J. DeKosky, M.J. Ernandes, I.S. Georgiev, H.J. Kim, M. Pancera, et al. NISC Comparative Sequencing Program. 2014. Developmental pathway for potent V1V2-directed HIV-neutralizing antibodies. *Nature.* 509:55–62. https://doi.org/10.1038/nature13036

Duty, J.A., P. Szodoray, N.Y. Zheng, K.A. Koelsch, Q. Zhang, M. Swiatkowski, M. Mathias, L. Garman, C. Helms, B. Nakken, et al. 2009. Functional anergy in a subpopulation of naive B cells from healthy humans that express autoreactive immunoglobulin receptors. *J. Exp. Med.* 206:139–151. https://doi.org/10.1084/jem.20080611

Flint, S.M., A. Gibson, G. Lucas, R. Nandigam, L. Taylor, D. Provan, A.C. Newland, C.O. Savage, and R.B. Henderson. 2016. A distinct plasmablast and naïve B-cell phenotype in primary immune thrombocytopenia. *Haematologica.* 101:698–706. https://doi.org/10.3324/haematol.2015.137273

Fritz, S., E. Mossdorf, B. Durovic, G. Zenhaeusern, A. Conen, I. Steffen, M. Battegay, R. Nüesch, and C. Hess. 2010. Virosomal influenza-vaccine induced immunity in HIV-infected individuals with high versus low CD4+ T-cell counts: clues towards a rational vaccination strategy. *AIDS.* 24:2287–2289. https://doi.org/10.1097/QAD.0b013e32833c6f92

Gianella, S., V. von Wyl, M. Fischer, B. Niederoest, M. Battegay, E. Bernasconi, M. Cavassini, A. Rauch, B. Hirschel, P. Vernazza, et al. Swiss HIV Cohort Study. 2011. Effect of early antiretroviral therapy during primary HIV-1 infection on cell-associated HIV-1 DNA and plasma HIV-1 RNA. *Antivir. Ther. (Lond.).* 16:535–545. https://doi.org/10.3851/IMP1776

Haas, A., K. Zimmermann, and A. Oxenius. 2011. Antigen-dependent and -independent mechanisms of T and B cell hyperactivation during chronic HIV-1 infection. *J. Virol.* 85:12102–12113. https://doi.org/10.1128/JVI.05607-11

Hammer, S.M., M.S. Saag, M. Schechter, J.S. Montaner, R.T. Schooley, D.M. Jacobsen, M.A. Thompson, C.C. Carpenter, M.A. Fischl, B.G. Gazzard, et al. International AIDS Society-USA panel. 2006. Treatment for adult HIV infection: 2006 recommendations of the International AIDS Society-USA panel. *JAMA.* 296:827–843. https://doi.org/10.1001/jama.296.7.827

Haynes, B.F., J. Fleming, E.W. St Clair, H. Katinger, G. Stiegler, R. Kunert, J. Robinson, R.M. Scearce, K. Plonk, H.F. Staats, et al. 2005. Cardiolipin polyspecific autoreactivity in two broadly neutralizing HIV-1 antibodies. *Science.* 308:1906–1908. https://doi.org/10.1126/science.1111781

Isnardi, I., Y.S. Ng, L. Menard, G. Meyers, D. Saadoun, I. Srdanovic, J. Samuels, J. Berman, J.H. Buckner, C. Cunningham-Rundles, and E. Meffre. 2010. Complement receptor 2/CD21- human naive B cells contain mostly autoreactive unresponsive clones. *Blood.* 115:5026–5036. https://doi.org/10.1182/blood-2009-09-243071

Jayaraman, S. 2003. Intracellular determination of activated caspases (IDAC) by flow cytometry using a pancaspase inhibitor labeled with FITC. *Cytometry A.* 56:104–112. https://doi.org/10.1002/cyto.a.10094

Kadelka, C., T. Liechti, H. Ebner, M. Schanz, P. Rusert, N. Friedrich, E. Stiegeler, D.L. Braun, M. Huber, A.U. Scherrer, et al. Swiss HIV Cohort Study. 2018. Distinct, IgG1-driven antibody response landscapes demarcate individuals with broadly HIV-1 neutralizing activity. *J. Exp. Med.* 215:1589–1608. https://doi.org/10.1084/jem.20180246

Kardava, L., S. Moir, N. Shah, W. Wang, R. Wilson, C.M. Buckner, B.H. Santich, L.J. Kim, E.E. Spurlin, A.K. Nelson, et al. 2014. Abnormal B cell memory subsets dominate HIV-specific responses in infected individuals. *J. Clin. Invest.* 124:3252–3262. https://doi.org/10.1172/JCI74351

Kernéis, S., O. Launay, C. Turbelin, F. Batteux, T. Hanslik, and P.Y. Boëlle. 2014. Long-term immune responses to vaccination in HIV-infected patients: a systematic review and meta-analysis. *Clin. Infect. Dis.* 58:1130–1139. https://doi.org/10.1093/cid/cit937

Kruetzmann, S., M.M. Rosado, H. Weber, U. Germing, O. Tournilhac, H.H. Peter, R. Berner, A. Peters, T. Boehm, A. Plebani, et al. 2003. Human immunoglobulin M memory B cells controlling Streptococcus pneumoniae infections are generated in the spleen. *J. Exp. Med.* 197:939–945. https://doi.org/10.1084/jem.20022020

Liao, H.X., R. Lynch, T. Zhou, F. Gao, S.M. Alam, S.D. Boyd, A.Z. Fire, K.M. Roskin, C.A. Schramm, Z. Zhang, et al. NISC Comparative Sequencing Program. 2013. Co-evolution of a broadly neutralizing HIV-1 antibody and founder virus. *Nature.* 496:469–476. https://doi.org/10.1038/nature12053

Liechti, T., H.F. Günthard, and A. Trkola. 2018a. OMIP-047: High-Dimensional phenotypic characterization of B cells. *Cytometry A.* 93:592–596. https://doi.org/10.1002/cyto.a.23488

Liechti, T., C. Kadelka, H. Ebner, N. Friedrich, R.D. Kouyos, H.F. Günthard, and A. Trkola. 2018b. Development of a high-throughput bead based assay system to measure HIV-1 specific immune signatures in clinical samples. *J. Immunol. Methods.* 454:48–58. https://doi.org/10.1016/j.jim.2017.12.003

Liu, M., G. Yang, K. Wiehe, N.I. Nicely, N.A. Vandergrift, W. Rountree, M. Bonsignori, S.M. Alam, J. Gao, B.F. Haynes, and G. Kelsoe. 2015. Polyreactivity and autoreactivity among HIV-1 antibodies. *J. Virol.* 89:784–798. https://doi.org/10.1128/JVI.02378-14

Lynch, R.M., L. Tran, M.K. Louder, S.D. Schmidt, M. Cohen, R. Dersimonian, Z. Euler, E.S. Gray, S. Abdool Karim, J. Kirchherr, et al. CHAVI 001 Clinical Team Members. 2012. The development of CD4 binding site antibodies during HIV-1 infection. *J. Virol.* 86:7588–7595. https://doi.org/10.1128/JVI.00734-12

Malaspina, A., S. Moir, S.M. Orsega, J. Vasquez, N.J. Miller, E.T. Donoghue, S. Kottilil, M. Gezmu, D. Follmann, G.M. Vodeiko, et al. 2005. Compromised B cell responses to influenza vaccination in HIV-infected individuals. *J. Infect. Dis.* 191:1442–1450. https://doi.org/10.1086/429298

Malaspina, A., S. Moir, J. Ho, W. Wang, M.L. Howell, M.A. O'Shea, G.A. Roby, C.A. Rehm, J.M. Mican, T.W. Chun, and A.S. Fauci. 2006. Appearance of immature/transitional B cells in HIV-infected individuals with advanced disease: correlation with increased IL-7. *Proc. Natl. Acad. Sci. USA.* 103:2262–2267. https://doi.org/10.1073/pnas.0511094103

Meffre, E., A. Louie, J. Bannock, L.J. Kim, J. Ho, C.C. Frear, L. Kardava, W. Wang, C.M. Buckner, Y. Wang, et al. 2016. Maturational characteristics of HIV-specific antibodies in viremic individuals. *JCI Insight.* 1:e84610. https://doi.org/10.1172/jci.insight.84610

Moir, S., and A.S. Fauci. 2009. B cells in HIV infection and disease. *Nat. Rev. Immunol.* 9:235–245. https://doi.org/10.1038/nri2524

Moir, S., and A.S. Fauci. 2013. Insights into B cells and HIV-specific B-cell responses in HIV-infected individuals. *Immunol. Rev.* 254:207–224. https://doi.org/10.1111/imr.12067

Moir, S., and A.S. Fauci. 2014. B-cell exhaustion in HIV infection: the role of immune activation. *Curr. Opin. HIV AIDS.* 9:472–477. https://doi.org/10.1097/COH.0000000000000092

Moir, S., J. Ho, A. Malaspina, W. Wang, A.C. DiPoto, M.A. O'Shea, G. Roby, S. Kottilil, J. Arthos, M.A. Proschan, et al. 2008. Evidence for HIV-associated B cell exhaustion in a dysfunctional memory B cell compartment in HIV-infected viremic individuals. *J. Exp. Med.* 205:1797–1805. https://doi.org/10.1084/jem.20072683

Moir, S., C.M. Buckner, J. Ho, W. Wang, J. Chen, A.J. Waldner, J.G. Posada, L. Kardava, M.A. O'Shea, S. Kottilil, et al. 2010. B cells in early and chronic HIV infection: evidence for preservation of immune function associated with early initiation of antiretroviral therapy. *Blood.* 116:5571–5579. https://doi.org/10.1182/blood-2010-05-285528

Moore, P.L., E.S. Gray, C.K. Wibmer, J.N. Bhiman, M. Nonyane, D.J. Sheward, T. Hermanus, S. Bajimaya, N.L. Tumba, M.R. Abrahams, et al. 2012. Evolution of an HIV glycan-dependent broadly neutralizing antibody epitope through immune escape. *Nat. Med.* 18:1688–1692. https://doi.org/10.1038/nm.2985

Moore, P.L., C. Williamson, and L. Morris. 2015. Virological features associated with the development of broadly neutralizing antibodies to HIV-1. *Trends Microbiol.* 23:204–211. https://doi.org/10.1016/j.tim.2014.12.007

Mouquet, H., J.F. Scheid, M.J. Zoller, M. Krogsgaard, R.G. Ott, S. Shukair, M.N. Artyomov, J. Pietzsch, M. Connors, F. Pereyra, et al. 2010. Polyreactivity increases the apparent affinity of anti-HIV antibodies by heteroligation. *Nature.* 467:591–595. https://doi.org/10.1038/nature09385

Nowicka, M., C. Krieg, L.M. Weber, F.J. Hartmann, S. Guglietta, B. Becher, M.P. Levesque, and M.D. Robinson. 2017. CyTOF workflow: differential

discovery in high-throughput high-dimensional cytometry datasets. *F1000 Res.* 6:748. https://doi.org/10.12688/f1000research.11622.1

Pape, K.A., J.J. Taylor, R.W. Maul, P.J. Gearhart, and M.K. Jenkins. 2011. Different B cell populations mediate early and late memory during an endogenous immune response. *Science.* 331:1203–1207. https://doi.org/10.1126/science.1201730

Pauken, K.E., M.A. Sammons, P.M. Odorizzi, S. Manne, J. Godec, O. Khan, A.M. Drake, Z. Chen, D.R. Sen, M. Kurachi, et al. 2016. Epigenetic stability of exhausted T cells limits durability of reinvigoration by PD-1 blockade. *Science.* 354:1160–1165. https://doi.org/10.1126/science.aaf2807

Portugal, S., C.M. Tipton, H. Sohn, Y. Kone, J. Wang, S. Li, J. Skinner, K. Virtaneva, D.E. Sturdevant, S.F. Porcella, et al. 2015. Malaria-associated atypical memory B cells exhibit markedly reduced B cell receptor signaling and effector function. *eLife.* 4:e07218. https://doi.org/10.7554/eLife.07218

Qiu, P., E.F. Simonds, S.C. Bendall, K.D. Gibbs Jr., R.V. Bruggner, M.D. Linderman, K. Sachs, G.P. Nolan, and S.K. Plevritis. 2011. Extracting a cellular hierarchy from high-dimensional cytometry data with SPADE. *Nat. Biotechnol.* 29:886–891. https://doi.org/10.1038/nbt.1991

Quách, T.D., N. Manjarrez-Orduño, D.G. Adlowitz, L. Silver, H. Yang, C. Wei, E.C. Milner, and I. Sanz. 2011. Anergic responses characterize a large fraction of human autoreactive naive B cells expressing low levels of surface IgM. *J. Immunol.* 186:4640–4648. https://doi.org/10.4049/jimmunol.1001946

Rakhmanov, M., B. Keller, S. Gutenberger, C. Foerster, M. Hoenig, G. Driessen, M. van der Burg, J.J. van Dongen, E. Wiech, M. Visentini, et al. 2009. Circulating CD21low B cells in common variable immunodeficiency resemble tissue homing, innate-like B cells. *Proc. Natl. Acad. Sci. USA.* 106:13451–13456. https://doi.org/10.1073/pnas.0901984106

Rieder, P., B. Joos, A.U. Scherrer, H. Kuster, D. Braun, C. Grube, B. Niederöst, C. Leemann, S. Gianella, K.J. Metzner, et al. 2011. Characterization of human immunodeficiency virus type 1 (HIV-1) diversity and tropism in 145 patients with primary HIV-1 infection. *Clin. Infect. Dis.* 53:1271–1279. https://doi.org/10.1093/cid/cir725

Roederer, M., L. Quaye, M. Mangino, M.H. Beddall, Y. Mahnke, P. Chattopadhyay, I. Tosi, L. Napolitano, M. Terranova Barberio, C. Menni, et al. 2015. The genetic architecture of the human immune system: a bioresource for autoimmunity and disease pathogenesis. *Cell.* 161:387–403. https://doi.org/10.1016/j.cell.2015.02.046

Rusert, P., R.D. Kouyos, C. Kadelka, H. Ebner, M. Schanz, M. Huber, D.L. Braun, N. Hozé, A. Scherrer, C. Magnus, et al. Swiss HIV Cohort Study. 2016. Determinants of HIV-1 broadly neutralizing antibody induction. *Nat. Med.* 22:1260–1267. https://doi.org/10.1038/nm.4187

Saadoun, D., B. Terrier, J. Bannock, T. Vazquez, C. Massad, I. Kang, F. Joly, M. Rosenzwajg, D. Sene, P. Benech, et al. 2013. Expansion of autoreactive unresponsive CD21-/low B cells in Sjögren's syndrome-associated lymphoproliferation. *Arthritis Rheum.* 65:1085–1096. https://doi.org/10.1002/art.37828

Sadlier, C., S. O'Dea, K. Bennett, J. Dunne, N. Conlon, and C. Bergin. 2016. Immunological efficacy of pneumococcal vaccine strategies in HIV-infected adults: a randomized clinical trial. *Sci. Rep.* 6:32076. https://doi.org/10.1038/srep32076

Saville, D. 2018. Multiple Comparison Procedures: The Ins and Outs. *In Applied Statistics in Agricultural, Biological, and Environmental Sciences.* B. Glaz and K.M. Yeater, editors. American Society of Agronomy, Madison, WI. 85–106. https://doi.org/10.2134/appliedstatistics.2015.0085

Schulz, K.R., E.A. Danna, P.O. Krutzik, and G.P. Nolan. 2012. Single-cell phospho-protein analysis by flow cytometry. *Curr. Protoc. Immunol.* Chapter 8:Unit 8.17.

Sciaranghella, G., N. Tong, A.E. Mahan, T.J. Suscovich, and G. Alter. 2013. Decoupling activation and exhaustion of B cells in spontaneous controllers of HIV infection. *AIDS.* 27:175–180. https://doi.org/10.1097/QAD.0b013e32835bd1f0

Segawa, K., S. Kurata, Y. Yanagihashi, T.R. Brummelkamp, F. Matsuda, and S. Nagata. 2014. Caspase-mediated cleavage of phospholipid flippase for apoptotic phosphatidylserine exposure. *Science.* 344:1164–1168. https://doi.org/10.1126/science.1252809

Seifert, M., M. Przekopowitz, S. Taudien, A. Lollies, V. Ronge, B. Drees, M. Lindemann, U. Hillen, H. Engler, B.B. Singer, and R. Küppers. 2015. Functional capacities of human IgM memory B cells in early inflammatory responses and secondary germinal center reactions. *Proc. Natl. Acad. Sci. USA.* 112:E546–E555. https://doi.org/10.1073/pnas.1416276112

Shirai, A., M. Cosentino, S.F. Leitman-Klinman, and D.M. Klinman. 1992. Human immunodeficiency virus infection induces both polyclonal and virus-specific B cell activation. *J. Clin. Invest.* 89:561–566. https://doi.org/10.1172/JCI115621

Subbaraman, H., M. Schanz, and A. Trkola. 2018. Broadly neutralizing antibodies: What is needed to move from a rare event in HIV-1 infection to vaccine efficacy? *Retrovirology.* 15:52. https://doi.org/10.1186/s12977-018-0433-2

Terrier, B., F. Joly, T. Vazquez, P. Benech, M. Rosenzwajg, W. Carpentier, M. Garrido, P. Ghillani-Dalbin, D. Klatzmann, P. Cacoub, and D. Saadoun. 2011. Expansion of functionally anergic CD21-/low marginal zone-like B cell clones in hepatitis C virus infection-related autoimmunity. *J. Immunol.* 187:6550–6563. https://doi.org/10.4049/jimmunol.1102022

Tipton, C.M., C.F. Fucile, J. Darce, A. Chida, T. Ichikawa, I. Gregoretti, S. Schieferl, J. Hom, S. Jenks, R.J. Feldman, et al. 2015. Diversity, cellular origin and autoreactivity of antibody-secreting cell population expansions in acute systemic lupus erythematosus. *Nat. Immunol.* 16:755–765. https://doi.org/10.1038/ni.3175

Titanji, K., A. De Milito, A. Cagigi, R. Thorstensson, S. Grützmeier, A. Atlas, B. Hejdeman, F.P. Kroon, L. Lopalco, A. Nilsson, and F. Chiodi. 2006. Loss of memory B cells impairs maintenance of long-term serologic memory during HIV-1 infection. *Blood.* 108:1580–1587. https://doi.org/10.1182/blood-2005-11-013383

Trkola, A., H. Kuster, C. Leemann, A. Oxenius, C. Fagard, H. Furrer, M. Battegay, P. Vernazza, E. Bernasconi, R. Weber, et al. Swiss HIV Cohort Study. 2004. Humoral immunity to HIV-1: kinetics of antibody responses in chronic infection reflects capacity of immune system to improve viral set point. *Blood.* 104:1784–1792. https://doi.org/10.1182/blood-2004-01-0251

Utzschneider, D.T., A. Legat, S.A. Fuertes Marraco, L. Carrié, I. Luescher, D.E. Speiser, and D. Zehn. 2013. T cells maintain an exhausted phenotype after antigen withdrawal and population reexpansion. *Nat. Immunol.* 14:603–610. https://doi.org/10.1038/ni.2606

Verkoczy, L., M. Diaz, T.M. Holl, Y.B. Ouyang, H. Bouton-Verville, S.M. Alam, H.X. Liao, G. Kelsoe, and B.F. Haynes. 2010. Autoreactivity in an HIV-1 broadly reactive neutralizing antibody variable region heavy chain induces immunologic tolerance. *Proc. Natl. Acad. Sci. USA.* 107:181–186. https://doi.org/10.1073/pnas.0912914107

Verkoczy, L., G. Kelsoe, M.A. Moody, and B.F. Haynes. 2011. Role of immune mechanisms in induction of HIV-1 broadly neutralizing antibodies. *Curr. Opin. Immunol.* 23:383–390. https://doi.org/10.1016/j.coi.2011.04.003

Walker, B., and A. McMichael. 2012. The T-cell response to HIV. *Cold Spring Harb. Perspect. Med.* 2:a007054. https://doi.org/10.1101/cshperspect.a007054

Ward, J.H. 1963. Hierarchical Grouping to Optimize an Objective Function. *J. Am. Stat. Assoc.* 58:236–244. https://doi.org/10.1080/01621459.1963.10500845

Wei, X., J.M. Decker, S. Wang, H. Hui, J.C. Kappes, X. Wu, J.F. Salazar-Gonzalez, M.G. Salazar, J.M. Kilby, M.S. Saag, et al. 2003. Antibody neutralization and escape by HIV-1. *Nature.* 422:307–312. https://doi.org/10.1038/nature01470

Weill, J.C., S. Weller, and C.A. Reynaud. 2009. Human marginal zone B cells. *Annu. Rev. Immunol.* 27:267–285. https://doi.org/10.1146/annurev.immunol.021908.132607

Wu, X., Z.Y. Yang, Y. Li, C.M. Hogerkorp, W.R. Schief, M.S. Seaman, T. Zhou, S.D. Schmidt, L. Wu, L. Xu, et al. 2010. Rational design of envelope identifies broadly neutralizing human monoclonal antibodies to HIV-1. *Science.* 329:856–861. https://doi.org/10.1126/science.1187659

Wyl, V., S. Gianella, M. Fischer, B. Niederoest, H. Kuster, M. Battegay, E. Bernasconi, M. Cavassini, A. Rauch, B. Hirschel, et al. Swiss HIV Cohort Study-SHCS. 2011. Early antiretroviral therapy during primary HIV-1 infection results in a transient reduction of the viral setpoint upon treatment interruption. *PLoS One.* 6:e27463. https://doi.org/10.1371/journal.pone.0027463

Zhang, L., Z. Li, Z. Wan, A. Kilby, J.M. Kilby, and W. Jiang. 2015. Humoral immune responses to Streptococcus pneumoniae in the setting of HIV-1 infection. *Vaccine.* 33:4430–4436. https://doi.org/10.1016/j.vaccine.2015.06.077

Zhang, R., L. Verkoczy, K. Wiehe, S. Munir Alam, N.I. Nicely, S. Santra, T. Bradley, C.W. Pemble IV, J. Zhang, F. Gao, et al. 2016. Initiation of immune tolerance-controlled HIV gp41 neutralizing B cell lineages. *Sci. Transl. Med.* 8:336ra62. https://doi.org/10.1126/scitranslmed.aaf0618